3-14-2014

# Positron Spectroscopy of Hydrothermally Grown Actinide Oxides

Edward C. Schneider


# POSITRON SPECTROSCOPY OF HYDROTHERMALLY GROWN ACTINIDE OXIDES

THESIS

Edward C. Schneider, Captain, USAF

AFIT-ENP-14-M-33

**DEPARTMENT OF THE AIR FORCE**
**AIR UNIVERSITY**

***AIR FORCE INSTITUTE OF TECHNOLOGY***

**Wright-Patterson Air Force Base, Ohio**

AFIT-ENP-14-M-33

# POSITRON SPECTROSCOPY OF HYDROTHERMALLY GROWN ACTINIDE OXIDES

THESIS

Presented to the Faculty

Department of Engineering Physics

Graduate School of Engineering and Management

Air Force Institute of Technology

Air University

Air Education and Training Command

In Partial Fulfillment of the Requirements for the

Degree of Master of Science

Edward C. Schneider, BS

Captain, USAF

March 2014

AFIT-ENP-14-M-33

# POSITRON SPECTROSCOPY OF HYDROTHERMALLY GROWN ACTINIDE OXIDES

Edward C. Schneider, BS
Captain, USAF

Approved:

| | |
|---|---|
| //signed// | 11 Mar 14 |
| James C. Petrosky, PhD (Chairman) | Date |
| //signed// | 11 Mar 14 |
| Larry W. Burggraf, PhD (Member) | Date |
| //signed// | 11 Mar 14 |
| Timothy W. Zens, Maj, USAF (Member) | Date |

## Abstract

In recent years AFIT has built expertise and resources dedicated to the growth and characterization of actinide oxides. The primary purpose of this research was to integrate positron spectroscopy – with which AFIT also has a long history – into this actinide research. The main objectives were to construct a Positron Annihilation Lifetime Spectroscopy system, including a new positron source, and to characterize a number of hydrothermally grown $ThO_2$ and U:$ThO_2$ crystals. Lifetime measurements were conducted on nine crystal samples and the spectra analyzed to determine the purity and quality of the crystals. In addition, analysis and fitting of the experimental data allowed estimates of contribution percentages to be made; the samples themselves account for less than 30% of the sample counts in all cases. Overall, the low resolution and large number of non-sample counts indicates that the system was not sufficient to characterize the crystals. A strong foundation for actinide PALS studies was laid, but further work is required to build a more effective system.

## Acknowledgments

I would like to extend my thanks to a number of people who helped with this thesis work: my advisor, Dr. Petrosky, and my committee members; Mr. Eric Taylor, Dr. David Turner, Dr. Justin Clinton, and Dr. Daniel Felker, for their advice and use of their equipment; Victrex Manufacturing, Ltd., for providing the polymer film used in constructing the T-134Q positron source; several ENP PhD students, particularly Dr. Tony Kelly, Maj Greg Van Dyk, and Maj Angelo Bonavita, for their invaluable assistance; my fellow ENP 14M students, especially MAJ Matthew Greb and Capt Jeff Graham, for their efforts and encouragement; and anyone else that I may have forgotten. Thank you.

Edward C. Schneider

# Table of Contents

Page

## List of Figures

# POSITRON SPECTROSCOPY OF HYDROTHERMALLY GROWN ACTINIDE OXIDES

## I. Introduction

### Background and Motivation:

This research is intended to be part of a larger Department of Defense effort to grow and analyze single-crystal actinide oxides. The work described here is an attempt to characterize the quality of crystals using positron annihilation spectroscopy (PALS). The crystal quality is heretofore unknown, since they are the first grown using hydrothermal (or Solvothermal) growth. PALS was performed on a number of crystal samples provided by AFIT. Some of these crystals have been previously characterized using other spectroscopic methods both at AFIT and at other institutions [1]; the PALS data should add to the body of knowledge regarding these materials, with the goal of finding a best method for quickly analyzing defect densities within actinide crystals. The principal reason for AFIT's interest in actinide oxides is their potential for use as highly efficient neutron detectors.

### Thesis Scope and Limitations

This thesis was confined to PALS analysis of nine actinide oxide crystals. The work entailed the construction and refinement of a new PALS system, the collection of data on each crystal, and the interpretation of those data.

There were several limitations on the overall scope of the project. Once the final configuration of the PALS apparatus was reached (after about four months), the time

spent collecting useful spectra was about 420 hours, or two and a half weeks – this limited the total number of detector events that were recorded. The samples themselves were subject to restrictions on drilling, cutting and other mechanical working, which restricted design choices for source placement. The safety considerations required for constructing a new positron source resulted in a larger positron emission region than required. The combination of large source area and small crystal size (especially for the uranium-doped thoria samples) resulted in recorded events that did not correspond to annihilations in the samples. The most important limitation was hardware-related; the oscilloscope used has a maximum sampling rate of 10 giga-samples per second (100-ps interval) when recording two channels. These limitations negatively affected the results of this research, but could be mitigated in a follow-on research effort.

**Thesis Content Summary**

This thesis document is split into three main sections and three appendices. Section II discusses relevant information on crystal growth and properties as well as briefly explains positron spectroscopy. Section III contains a detailed description of how and why the experimental apparatus was constructed, as well as a discussion of the data characteristics and analysis techniques. Section IV presents the results gleaned from this thesis research, including some unexpected phenomena. Section V provides a concluding discussion and offers recommendations for future work. Appendix A is a listing of all the components of the PALS system, including model number, serial number, and settings. Appendix B lists the data sets used to generate the results presented in Section IV.

Appendix C is the documentation of the procedure used to assemble the T-134Q positron source used in this research.

## II. Theory

### Crystal Structures and Defects:

Very pure materials that solidify under carefully controlled conditions conform to a characteristic crystal lattice configurations. That is, the atoms of which the material is composed will arrange themselves in a repeating pattern with long-range order if the conditions are right. The exact arrangement of these atoms depends on many factors; chief among them being atomic radius and ionization state (in an ionic solid). Due to the wide range of values for these properties – even among compounds containing the same element – there are many possible lattice configurations. For most crystals, the pattern is some variation of an infinite series of cubes, rectangular prisms, or hexagonal prisms. Perfect $ThO_2$ crystals have a type of cubic lattice[1].

Of course, materials rarely form perfect crystals. Any number of factors can induce defects within the material, including regions with differing stoichiometry, rapid cooling, or impurities present during solidification. If the goal is to produce pure, mono-crystalline materials, any of these defects will be a drawback. However, when creating semiconductor devices, defects and especially impurities may be desirable as they can change both the mobility of charge carriers and their population [2].

It is important to understand some specific types of defects to properly interpret spectroscopy data. The primary focus of this research is vacancy defects. These typically result when rapid growth of the crystal leaves some gaps in the lattice or along the boundary when multiple crystals grains grow next to one another. This is shown in Figure 1.

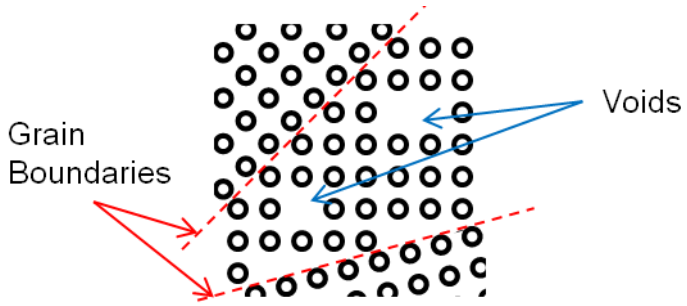


**Figure 1: Voids and grain boundaries in a material's lattice structure.**

These gaps are regions of lowered electron density, which will be critical to the interactions of positrons with the matter. Other types of defects that would be likely to be present in these materials are interstitial atoms and substitution defects. These result when an atom is incorporated in between the spaces in the lattice (interstitial) or when some other element – possibly an impurity - substitutes for an atom of the base material. Interstitial atoms may also be impurities; this is the basis for many metal alloys [2].

**Actinide Oxides:**

Some materials of particular interest are oxides of certain heavy metals in the actinide group of the periodic table. The metals themselves have many useful properties; in particular, they have isotopes that are easily fissioned. This is, of course, the basis of nuclear power generation and of nuclear weapons technology. Actinide metals are used in nuclear weapons and in some special reactors. Actinide oxides are used as fuel in most nuclear reactors because of their high melting temperatures (thousands of Kelvin) and chemical stability. Most commonly, these are uranium oxide, though thorium oxide and other blended fuels are also in use [3].

Oxide fuels are traditionally in the form of a sintered pellet. Sintering is the process of heating and compressing a powder of a material (with initial grain sizes typically in the 50-500 μm range) so that the atoms migrate to contact areas between the powder grains, lowering their total surface area and interconnecting the grains. A diagram of this process is shown in Figure 2. Sintered material generally has a large number of pores in the 1-10 μm range, lacks mechanical strength, and is a poor conductor of heat and electricity. These properties often lead to the fracturing of sintered fuel pellets, which may exacerbate their poor qualities [2].

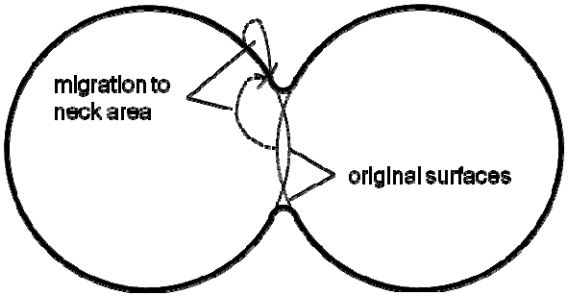


**Figure 2: The sintering process. At elevated temperature and pressure, material diffuses to form a neck between particles, lowering the overall energy of the system.**

Single-crystal actinide oxides have several properties that are superior to sintered pellets with regard to operation within a nuclear reactor. Single crystals are immensely strong and temperature resistant. Although degradation through accumulation of fission products is a concern, the relatively open crystal lattice of actinide oxide crystals provides sites to accommodate these products. Single crystals also have improved thermal conductivity, which could either simplify reactor design by allowing them to run at a higher core temperature for increased efficiency or have higher emergency temperature margins. Actinide oxide crystals are semiconductors with a very useful band gap,

similar that of to silicon's. Semiconductivity may offer a novel way to monitor the fuel elements in a reactor, but would also allow the construction of electrical devices based on the actinides themselves. These devices could be intrinsically radiation-hard, or they could capitalize on the large neutron cross-section of certain isotopes in order to create extremely efficient neutron detectors [1][2].

**Hydrothermal Growth:**

The high melting temperature of actinide oxides makes them very difficult to grow using common techniques. For example, the Czochralski method is commonly used to create high-purity single-crystal silicon, and requires a melt temperature of about 1700 K. To make uranium oxide via the same process, the melt would have to be at about 3150 K, which would destroy the quartz crucibles employed in silicon growth ($T_m$ = 1950 K) [4].

The hydrothermal (or Solvothermal, if a solvent other than water is used) growth process allows one to avoid operating a system at prohibitively high temperatures. Hydrothermal growth is commonly used to grow high-temperature crystalline materials, especially commercial quantities of pure quartz. In this method, the powdered material is placed in a solution which contains extremely powerful mineralizers, such as cesium fluoride for actinide oxide growth, at a high concentration. A seed crystal is suspended above the solution, and both the solution and seed are sealed in an autoclave. The lower region of the autoclave is heated to a point where the solution can dissolve the powdered material, while the upper region is maintained at a lower temperature where the material will precipitate out of solution. The growth apparatus is shown in Figure 3 [1].

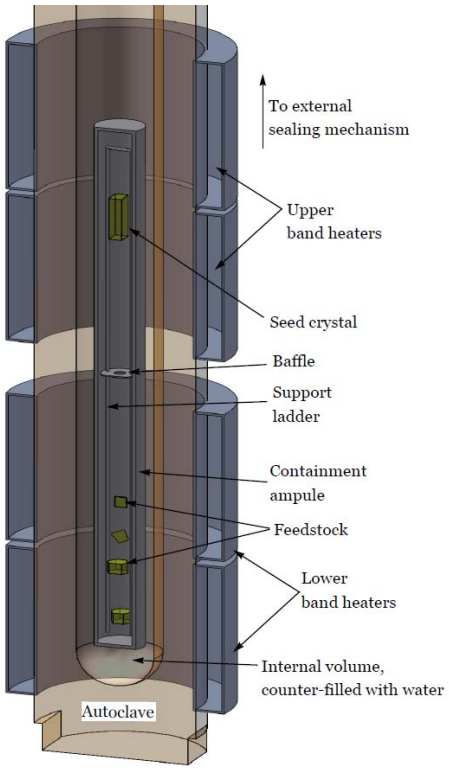


**Figure 3: A cutaway diagram showing a typical hydrothermal growth system. From Graham [5].**

Temperatures in the range of 600-1000K are required, which generates high pressures of 90-130 kPa that must be contained by the autoclave. The temperature gradient causes convective flow of the saturated solution upwards into the cooler zone, where it is super-saturated and the material will attempt to precipitate. The seed crystal provides a site for precipitation, which in turn will cause it to grow [1].

Hydrothermal growth is not without potential drawbacks. Due to the extremely harsh environment within the autoclave, monitoring in-situ growth is not possible at this time. It is also necessary to use some kind of capsule or liner made of a non-reactive precious metal (e.g. silver or platinum) in order to protect the pressure vessel; the cost of these metals is not insignificant. The process can take quite a long time, since overly

rapid crystal growth will result in defects – combined with the inability to monitor the reaction, this may lead to weeks wasted on unsuccessful growth runs. The other chemicals in the solvent and any impurities in the stock material may incorporate into the newly grown crystal or even dissolve through the seed crystal. This is particularly troublesome if the assembly is cooled rapidly resulting in solid condensation on the crystal, which is commonly referred to as "crashing out." A minor issue is that the seed crystal must be suspended somehow. Normally this involves drilling a hole and running a wire through it. The wire may cause problems with analytical techniques if it is left in the crystal, and some materials require special considerations when drilling. The crystals used in this research were spontaneously nucleated and grew on the walls of the reaction vessels, so they have no holes or wires in them [1].

**Positron Annihilation Spectroscopy:**

A particle with the same mass as the electron, but a positive charge, was predicted mathematically in 1928. Tracks corresponding to such a particle were noticed in cloud chamber experiments in 1932, and later came to be known as the positron. During the 1940s and 1950s, early experiments using electron-positron annihilation to characterize materials' electronic characteristics were conducted. These were the first uses of Positron Annihilation Spectroscopy (PAS), a suite of techniques that depend on the interactions of positrons with normal matter in order to gain some information about the structure of a test sample. All of these techniques depend on the property that the positron is the antimatter complement of the electron, and at meV energies – such as following thermalization within a solid material – the two will annihilate upon colliding

with one another. This annihilation will result in the emission of gamma radiation, and the characteristics of this radiation offer information about the conditions under which the annihilation occurred. Most positron spectroscopy techniques require a large number of events to provide statistically useful data [6].

Positron annihilation in condensed matter generally results in the emission of two 511 keV gamma photons in approximately opposite directions. However, annihilation in materials with regions of lowered density can result in the emission of more than two gamma photons. These photons still share the total 1.02 MeV energy between them, and will likely be emitted without the colinearity (or near-colinearity) that characterizes two-gamma emission, as shown in Figure 4.

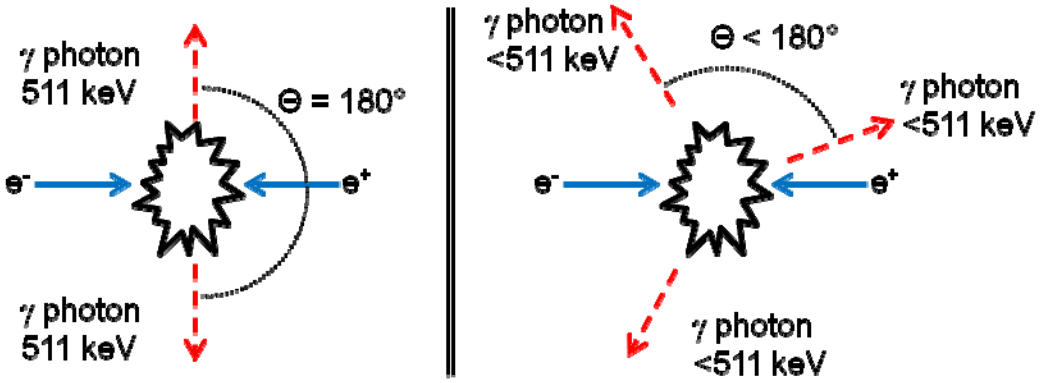


**Figure 4: 2-gamma and 3-gamma emission due to electron-positron annihilation.**

This is the basis of 2-gamma/3-gamma spectroscopy. In short, if the energy of emitted photons is measured to be significantly less than 511 keV, it can be surmised that the annihilation took place in a region of low density. Alternately, if two or more photons from a single event are measured with a large deviation from colinearity, the same conclusion may be valid. While this method can be used to characterize vacancy

populations in some materials (since vacancies are low-density regions), the small size of the crystal samples makes it difficult to ensure annihilations take place within them [6].

Assuming that only 2-gamma events are significant still leaves several PAS techniques available for analysis of $ThO_2$ crystals. If the electron that participates in the annihilation was bound to an atom in the material, its angular momentum will confer detectable components to the gamma radiation. This idea is fundamental to the Doppler broadening of annihilation radiation (DBAR) and angular correlation of annihilation radiation (ACAR) spectroscopy methods. In short, the component of angular momentum parallel to the gammas will result in a slight Doppler shift in the radiation, while the component perpendicular to the gammas will result in a deviation from perfect colinearity; that is, the gamma radiation will be slightly more or less than 511 keV and slightly more or less than 180° apart. Figure 5 shows a conceptual comparison between the three techniques.

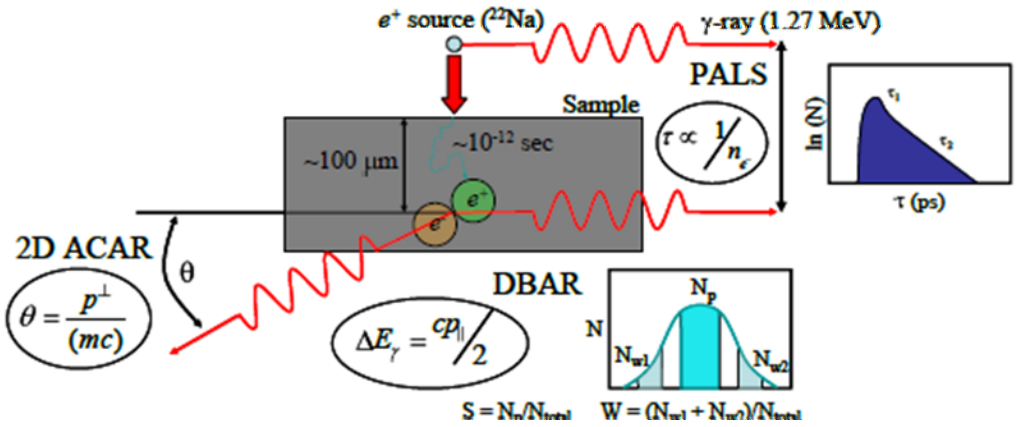


**Figure 5: Comparison of ACAR, DBAR, and PALS. From Williams [7].**

DBAR and ACAR are useful for characterizing material defects, and especially for identifying impurities in the sample (whose electron configurations will differ from the expected elements). This research did not use DBAR or ACAR, but AFIT will soon have a powerful capability to perform these measurements in the form of a slow positron beam. Future work incorporating electron momentum characterization would be very valuable [6].

Another common PAS technique is positron annihilation lifetime spectroscopy (PALS). PALS systems record the time between the emission or injection of a positron and its annihilation. This may be done using very well-timed beam systems whose pulse timings and pulse widths are controllable within tens of picoseconds, for reasons that will become obvious. PALS is much more commonly implemented using a sample of a positron-emitting isotope placed in contact with the sample, avoiding the need for the electromagnetic coils and electronics of a beam system. In most cases, the isotope that acts as a positron source is sodium-22, which has a relatively short half-life (2.6 y) and emits a characteristic gamma photon (at about 1.28 MeV) simultaneously with a positron upon nuclear decay to neon-22. Using this decay gamma as a start signal, it is then possible to wait for a 511 keV gamma that signals the annihilation of the positron, which will commonly occur between 100 and 500 ps later. The lifetime of positrons in a material is chiefly determined by the material's electron density. More electronically dense materials, such as metals, have short average lifetimes, while semiconductors and many ionic compounds have longer lifetimes because the electrons are more tightly bound. However, vacancies and voids in the material provide regions in which positrons may become trapped and survive relatively longer. If, for example, silicon crystals

normally have a positron lifetime of 200 ps, defects may have a positron lifetime of 300-500 ps. Therefore, if the baseline lifetime for a given material is known, an estimate of the vacancy population can be made based on the lengthening of the average positron lifetime. This principle is the foundation for the PALS experiments conducted during this thesis work [6].

# III. Methodology

## Overview

This section will discuss the methods by which experiments were conducted in this thesis research It is divided into two main parts. The first part describes the physical assembly of the test apparatus, including an explanation for a number of design decisions. The second part describes the properties of the data that was collected and the analysis techniques applied to them. A concise overview of the whole process from positron emission to data fitting is presented at the end of the section.

## Experiment Setup

The equipment required to perform Positron Annihilation Lifetime Spectroscopy (PALS) is not particularly specialized. There are two major considerations for any PALS device. The setup should minimize positron interactions with anything other than the sample being examined, and the time resolution should be as high as possible. The equipment's count rate is also important, but longer count times may substitute for higher count rate when using an isotope that is long-lived compared to the experiment time, as is the case in this research.

### *Minimizing extraneous interactions:*

Minimizing positron interactions with matter other than the sample requires engineering trade-offs. While the initial impulse may be to conduct PALS in a vacuum vessel, this adds greatly to the complexity of the overall setup due to additional hardware requirements (vessel, pumps, etc.), additional material considerations (e.g., outgassing concerns), and additional time for vessel depressurization. This somewhat defeats the

advantage of simplicity offered by PALS. Instead, one simply recognizes that air has a much lower electron density than most solids or liquids, which are the commonly the test objects for PALS and accept some extraneous counts from air interactions. Practically, the air contribution to annihilation lifetime has a $\tau$ of about 500 ps, which is greater than the positron lifetime in most solids, which range from 120 to 350 ps [6].

In the initial setup, the detectors were simply located on a lab bench with much solid material within range of the positrons, The first coincidence tests actually had the positron source held up by a sheet of lead. It was quickly realized that these materials were generating a large number of annihilation counts. An intermediate experiment was designed using a small polystyrene (PS) shelf to hold the sample. However, extraneous interactions were still probable in the shelf, the shelf support, and laboratory bench. Therefore, the spectrometer was re-configured to maximize air space around the sample and minimize the solid angle subtended by the solid structural materials required to hold the samples and the detectors. This was accomplished by suspending the sample stage and sensors above the bench using standard chemistry laboratory stands. The sample stage was about 50 cm above the lab bench, which was deemed necessary because there was almost no material between the Na-22 source and anything below the stage. The progression of source-sample geometries is shown in Figure 6.

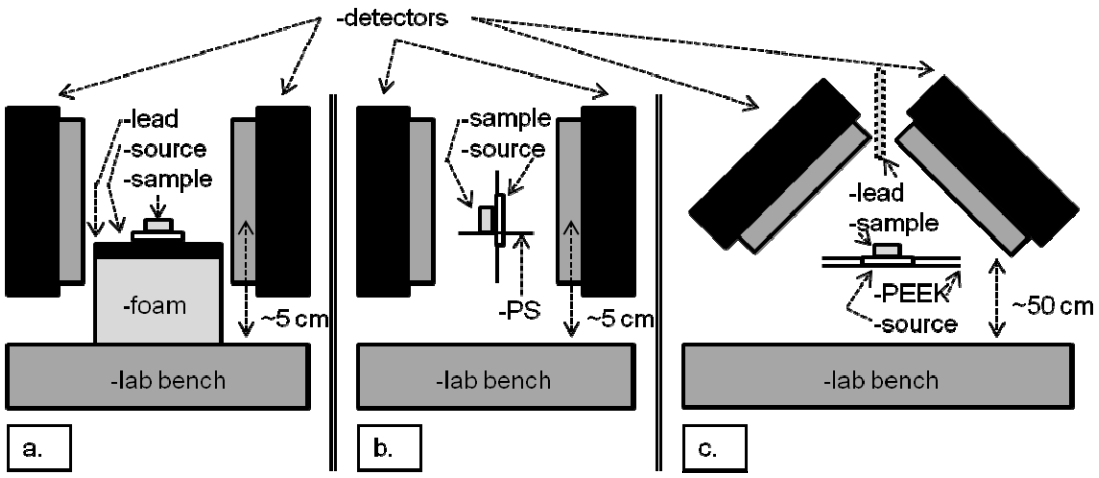


**Figure 6: Different source-sample geometries that were used during this research: (a) initial setup with lead plate right next to the source, (b) intermediate setup with PVC shelf but co-linear detectors and close to lab bench, and (c) final setup with elevation above lab bench, detector angling, PEEK sandwich source, and (out-of-plane) lead shield between detector crystals.**

A Na-22 sandwich source was constructed to maximize the number of annihilations in the test sample. Two 8 um-thick sheets of polyether ether ketone (PEEK) polymer contained the Na-22 salt left over from the evaporation procedure described in Appendix C. This polymer was selected over a simple polyvinyl chloride (PVC) sheet due to its high strength, demonstrated impermeability to water, and high working temperature (desired for the evaporation procedure) – a PVC sheet would have to have been much thicker to meet these requirements. PEEK contains hydrogen, carbon, and a very small amount of oxygen, which is a welcome, though not critical, advantage over the more electron-dense PVC. The PEEK sheets were held in a plastic frame made of high density polyethylene, which contains only hydrogen and carbon. Other materials that were more than 0.5 cm from the Na-22 but closer than 2 cm included: adhesive tape in the source frame, standard white paper for the stage, and nylon thread suspending the

stage. All of these are plastics or organic materials, and have low electron density. Their combined mass was no more than 0.6 g.

The closest high electron density material within range of the positrons was the sheet of lead placed between the two detectors. This was necessary to reduce environmentally triggered background counts and it subtends a very small solid angle with respect to the detector. Thus, the benefit of the lead sheet outweighs the potential noise that it introduces. The only other material that was closer to the stage than the $BaF_2$ detector crystals was the aluminum from the protective cover surrounding the detectors.

***Achieving useful time resolution:***

The electronics of most PALS systems, including those constructed previously at AFIT, follow a standard configuration. An example is shown in Figure 7(a). Many aspects of this standard setup were modified for the spectrometer constructed as part of this thesis project, which is shown schematically in Figure 7(b) and in the photograph in Figure 8.

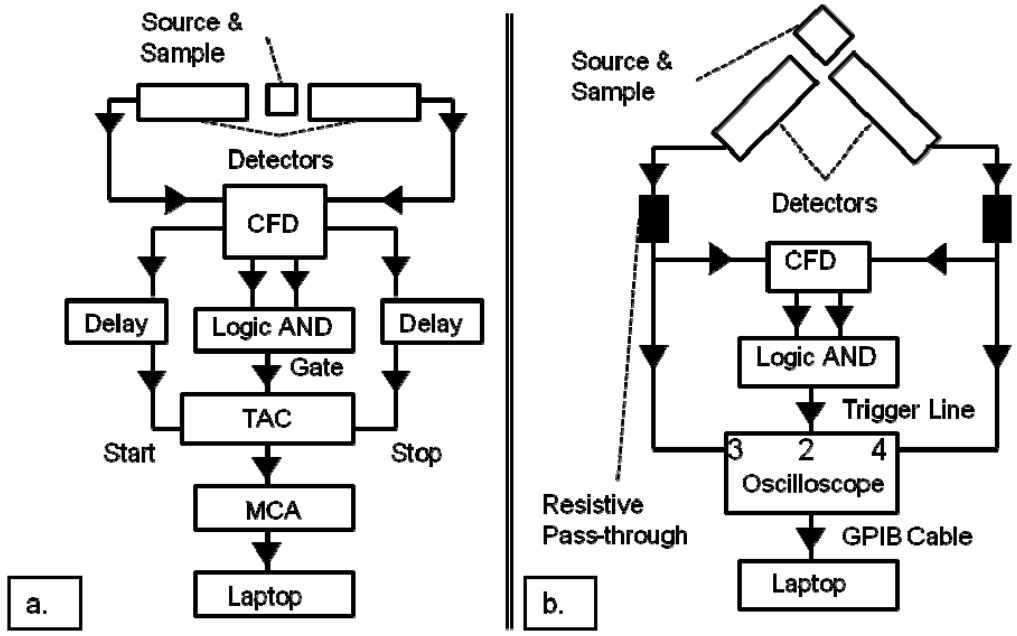


**Figure 7: A comparison of PALS systems in block diagram format. (a) The TAC-based system used by Williams [7]. (b) The oscilloscope-based system used in this research. Similiarities include the use of a CFD and logic box. Differences include the detector placement angle and use of an oscilloscope as opposed to a TAC and MCB combination.**

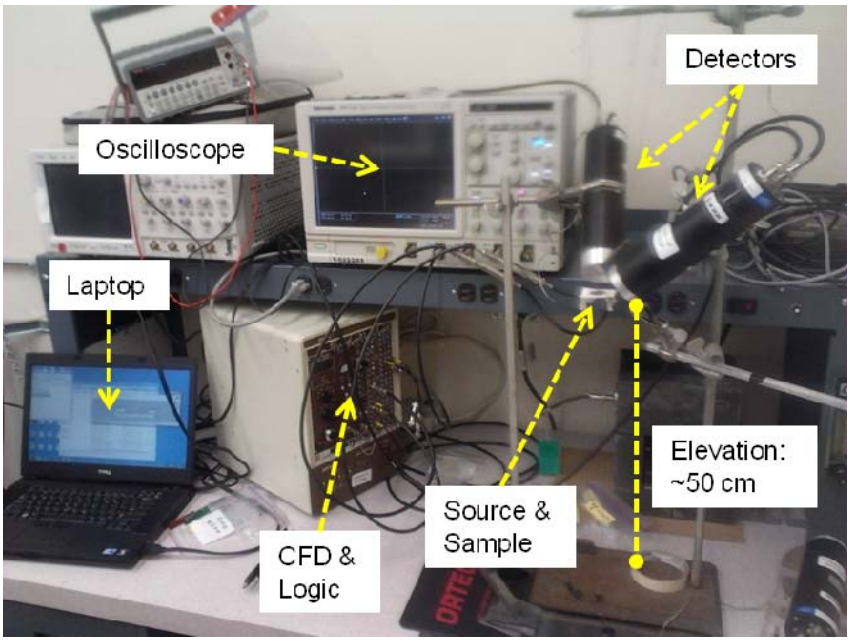


**Figure 8: Labeled photograph of the PALS system used for this research.**

In order to maximize annihilations in the sample, many PALS systems surround the positron source with sample material. This can be accomplished by immersing a source in the sample, drilling a hole into it and inserting a source, or using two pieces of the sample material and sandwiching the source between them, as shown in Figure 9(d). For this thesis, the goal was comparative spectroscopy on similar but distinct samples. Using two samples at once would have defeated the purpose of the analysis. Unless the crystals could have been cut in half, which was not possible due to restrictions on the mechanical processing of radioactive materials, the source could only be placed adjacent to the crystal. An intermediate design included a set of small clamps to hold the positron source vertically, with the crystal placed on a small stage of polystyrene directly adjacent to it as shown in Figure 6(b). This was rejected because of it induced extraneous interactions and because the crystal would often move off of center or even drop off of the stage. In the final configuration, the Na-22 source was incorporated into the stage below the sample, as shown in Figure 6(c) and Figure 9(f). This also allowed the sample to be "mounted" just by placing it on the stage (as shown in Figure 9(f)), removing any need for adhesive that might leave a residue on the crystal. The stage was suspended by threads from a ring stand far enough above it so that positron interactions were inconsequential, and the threads, having both low electron density and negligible solid angle were chosen to reduce background and unwanted positron interactions.

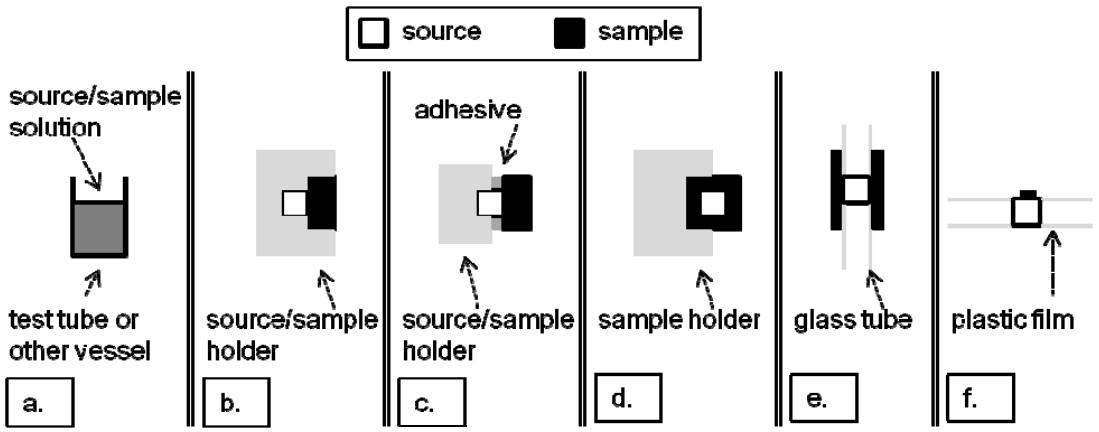


**Figure 9: Some possible PALS sample/source geometries. (a) Sample intermixed with source, (b) source and sample mechanically fixed into a mount, (c) source/sample adhered to a mount, (d) source encased or surrounded by sample, (e) sample deposited on the outer surface of a source container, (f) sample placed on a flat surface containing the source. This research used the arrangement shown in (f), because it works well with irregular samples and minimizes the amount of extra material.**

The detectors used in this research are scintillation-based gamma-ray detectors. Each one consists of a solid barium fluoride crystal that is connected to a photo-multiplier tube (PMT). When a gamma photon deposits energy in the crystal, the crystal responds with photon emissions of lower energy (scintillation). When these photons strike a photocathode at the back face of the crystal, it ejects electrons into the PMT. The PMT maintains several amplifier stages at high voltage, which accelerate the incoming electrons causing an avalanche of more electrons in each of the PMT stages, eventually resulting in a current output signal at the end of the tube.

Detector geometry and triggering is key, since PALS is based upon a coincidence timing measurement. Originally the detectors were placed in a co-linear configuration, which increases their solid angle greatly; but the drawback is that they can trigger on the dual 511 keV gammas radiating from a single annihilation event. The detectors in this experiment were placed at approximately a 90° angle in order to prevent this; there was

no co-linearity between any part of the $BaF_2$ crystals and the sample. An alternate method to prevent the 511 keV gamma from starting the trigger is to perform energy discrimination on start events. This was deemed unfeasible with the detectors that were used because there was little difference between the waveforms corresponding to different energy events. This is shown in Figure 10.

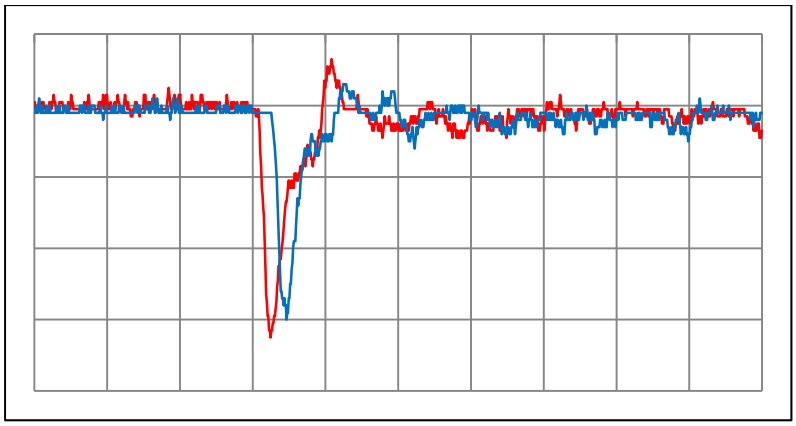

**Figure 10: Representative waveforms captured from an oscilloscope after detector events. The left peak (red trace) is the start signal from a 1.28 MeV gamma photon. The right peak (blue trace) is the stop signal from a 511 keV gamma photon. Note that the shapes of the two signal traces are nearly indistinguishable.**

Many PALS systems use dedicated start and stop detectors, but some can trigger off of multiple detectors. This thesis research used multiple start detectors in order to maximize the solid angle for start photons. Almost all PALS systems (including the one used in this thesis) then route detector signals into a constant-fraction discriminator (CFD) to generate logic pulses.

Collection of timing data is the principal area in which the PALS system employed in this thesis differs from most others. The conventional method, as in Figure 7(a), is to run the start and stop signals into a time-amplitude converter (TAC), which

outputs a voltage that corresponds to the delay between the two signals. This voltage is then fed into multi-channel analyzer (MCA) which then outputs data into "bins" that correspond to the lifetimes exhibited by individual events. There are a few issues with this approach. The timing difference in PALS is on the order of 100-200 ps, which is very fast for a TAC alone to register. The output signal representing the timing is not visible below the electronic noise floor of 15-20 mV and may be undetectable. The obvious solution is to implement a delay line, which creates a baseline amplitude onto which the extra amplitude from the birth-annihilation timing is added (and also serves to ensure that the TAC is in its linear response region). However, it was discovered early in this research that the TAC output waveform is not smooth; there are small amplitude oscillations at the top it. These oscillations on top of the delay-amplitude output pulse are of a greater magnitude than the timing differences that needed to be measured, preventing a timing difference calculation of less than ~100 ps. Therefore, another time difference scheme had to be found.

Instead of using the TAC/MCA method, this research employed the oscilloscope-based PALS system shown in Figure 7(b). The two signals (birth and annihilation) were converted into logic pulses by the CFD and fed into a logic "AND" circuit to obtain coincidence. That logic pulse was used as an input trigger, which signaled the oscilloscope to record the two signal waveforms separately in memory. A LabView script was then used to collect the waveform data and reset the oscilloscope. This method generated a larger data set than the TAC/MCA method (hundreds of MB per day). A potential disadvantage is the loss of data during dead time if the activity of the source was too great as the maximum count rate was ~10,000 counts per hour. However, the data

had two advantages over other methods. First, the signal sampling rate was only constrained by the oscilloscope's internal clock; in this work, one sample per 100 ps. This meant that faster oscilloscopes would have generated higher-resolution data (unfortunately no such device was available for this work). Second, the signal waveforms from the $BaF_2$ detectors are recorded directly, which allows for any amount of post-collection analysis to include interpolation or visual inspection.

***Increasing counts and count rates:***

There are many ways to increase the number of counts from a given experimental setup. For example, a researcher might increase the detector solid angle, use a larger activity source, or increase the measurement time. Each of these three methods was used during the design of the PALS system used in the current research. These factored in the construction of the "trapeze" arrangement as described previously, the construction of the T-134Q source, and the choice of an average of ~24 hours of count time per crystal.

The result was a count rate of approximately 500 counts per hour, yielding approximately 12,000 total counts per sample. It should be noted that most PALS systems collect anywhere from $10^6$ to $10^8$ counts per sample, two to four orders of magnitude more than this research. The implications of this low data number will be discussed in the analysis section, but it is worth noting that simply extending count times is not likely to result in the quality of information found in other research. Future researchers may wish to find other ways to increase their total counts, such as creating a more active positron source.

**Experiment Operation:**

The methods and parameters used for operating the PALS system are crucial to evaluating the data that are produced. The device model numbers and serial numbers are provided in Appendix A, along with specific settings for the equipment. It is worth noting that this final setup was the result of months of trial-and-error testing. Appendix A is provided as much for validation as to save future researchers some of this effort. AFIT has had numerous PAS instruments built and disassembled over the past decade and an ancillary goal of this thesis was to provide sufficient information that a PALS system could be easily reconstructed for use with actinide crystals if necessary.

Once the components were assembled and powered on, background measurements were garnered with no radioactive source on the stage. This was followed by a baseline measurement with just the T-134Q PEEK sandwich source, then another using a copper sheet. After these initial measurements were obtained, individual crystals were placed on the stage, and at least 10,000 counts obtained for each sample. The significance of these measurements will be discussed in Section IV.

**Data Analysis Methodology**

***Data characteristics***

Due to the balance of collection time and the activity of the source developed, several thousand counts were obtained for each crystal sample. The exact numbers are given in Appendix B. Each of these "counts" is actually a data file captured from the oscilloscope containing signal waveforms from both detectors. The amount of disk space required to record this data is not inconsequential; well over six gigabytes. If the

measurements were expanded to include approximately one million counts per sample, each measurement would require ~ 40 GB of storage space. This may be an important consideration for any future work using this method.

The data files are not particularly complex; each is a comma-separated-value (.csv) file containing two columns of one thousand voltage measurements with three header lines. Each row of the file represents the oscilloscope measurement of the voltage at 100 ps increments.

This 100 ps sampling increment is central to analysis of the data. It results from hardware limitations of the oscilloscope. The scope has four internal clocks that correspond to its four input channels. Each of these clocks allows a maximum sampling rate of 5 GHz, which leads to a nominal 200 ps sampling increment. However, if less than four channels are used, the scope will interleave its clocks to allow for a faster sampling rate. This allows 10 GHz sampling for two channels simultaneously or 20 GHz sampling for a single channel. However, a solution could not be found that allowed the recording of both sensor signals on one channel, so 10 GHz was the maximum sampling rate achievable. While it is theoretically possible to use two oscilloscopes to obtain a 20 GHz sampling rate, this adds a great deal of complexity since the scopes' clocks must be synchronized, two laptops would be needed, the data files would have to be merged in post-processing, and there may be added error due to drift in the clocks. These additional challenges were deemed too great to be implemented for this research.

***Lifetime values and interpolation, schemes***

While a 100 ps sampling increment is more than sufficient for many applications, it alone is not sufficient for PALS analysis. This is because of the extremely short

lifetime of positrons in solids. While lifetime is dependent on material density, even gaseous matter will cause annihilations within approximately 500 ps. In condensed states, average positron lifetimes generally range between 100 and 300 ps. Some sample relevant lifetimes are listed below:

| **Material** | **Average positron lifetime, $\tau$** |
|---|---|
| Air [6] | ~ 500 ps |
| Metal (copper) [6] | ~ 150 ps |
| Semiconductor (Si) [6] | 218 ps |
| Sintered $ThO_2$ pellet [8] | 184 ps |

Clearly, some method for obtaining better time resolution is needed. This may be achieved by using a very large number of counts, which is how a TAC-based system can overcome the inherent low sensitivity in its electronics. However, the data collection method used in this research preserves waveform data, which allows for interpolation. By interpolating the signal rise data, it is possible to achieve an estimate for the time of photon interaction that lies between the 100 ps sample points.

For example, consider the period between the time when a signal rises out of the noise floor and when it reaches its peak. If this region contains ten data points, one can use some of those to perform an interpolation. A linear interpolation model might miss the last few points before the peak (when the signal is turning over) to draw a line that intersects the zero axis or the noise floor. Since noise is not a constant value in all data files, it is simpler just to intersect at zero when using a linear interpolation. This intersection can be subtracted from the intersection point obtained for the other signal

waveforms to yield a delay between the two. A diagram illustrating how this simple linear interpolation was applied to sample traces is shown in Figure 11.

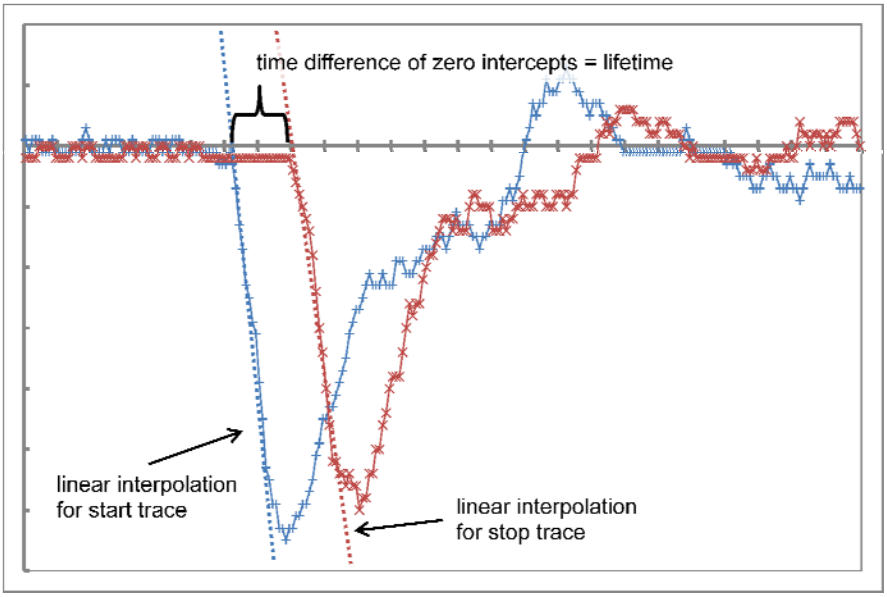


**Figure 11: An example of a linear interpolation scheme used in this research.**

Other interpolation schemes are possible as well, depending on how the signal is modeled. The real rise time behavior of the detector is approximately exponential in nature, though actually describing the waveform with exponentials is difficult due to the interference of atomic and electronic noise. Previous researchers [9] have attempted to model the behavior of deposition using the leading edge of a Gaussian function, and during the course of this thesis other models were also considered. However, because of the discrete nature of the data capture, attempting to use a higher binning shows that the points still cluster around the initial 100 ps increment points. This clustering also means that using a bin size that does not divide evenly into the sample increment shows odd spikes where the bins line up, as shown in Figure 12. As a result of these factors, the

lifetime differences were simply found from the raw data rather than interpolated data. Finally, the expected maximum resolution of this apparatus under any post-processing is around 100 ps.

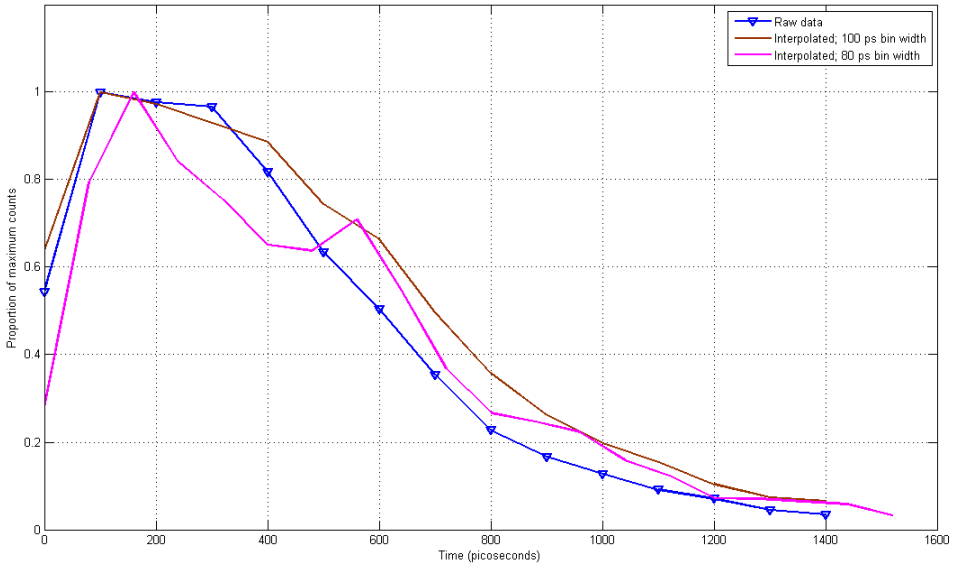


**Figure 12: Plots showing the effect of interpolated data clustering around un-interpolated values. The curve with two peaks is more tightly binned, and the second peak is caused by alignment in bins rather than any real phenomenon.**

Once positron lifetimes have been determined for each data point in a set, they must be collected and binned to form a histogram plot. For a TAC-based PALS system, this is accomplished by the MCA unit and the results generally follow that in Figure 13. For this research, the histogram is created in the same MATLAB script that performs interpolation of the data files, and looks something like Figure 14. The general shape is a sharp rise followed by an exponential decay. This indicates a short lifetime for the majority of positrons (~100 ps). Positrons with longer lifetimes are those which have traversed areas with less electron density, either due to the intrinsic material properties or

because they have been trapped in a vacancy. These longer-lived electrons form the tail of the lifetime distribution, with a 'fatter' tail indicating a longer average lifetime.

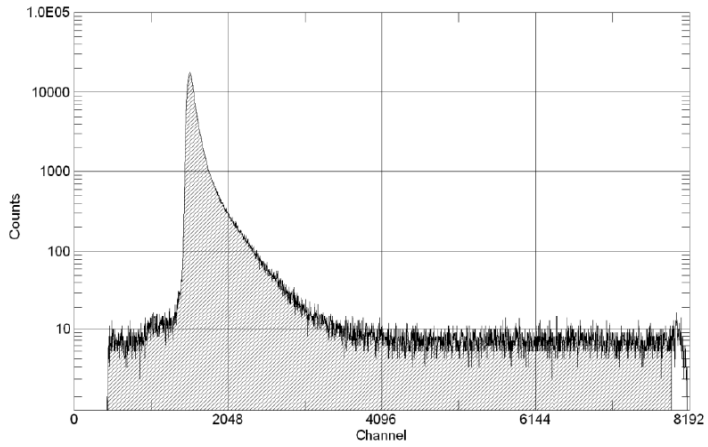


**Figure 13: A representative PALS spectrum taken with a TAC/MCA system. Note the extremely fine binning of tens of picoseconds. [7]**

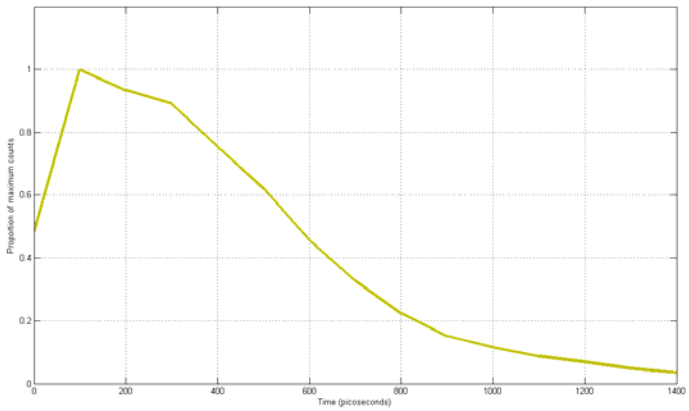


**Figure 14: A representative PALS raw data spectrum with the oscilloscope direct-capture system. Note the coarse binning based on sampling interval.**

As shown in Figure 14, the experimental system in this work does not generate data that are as clearly defined as those generated by using PALS techniques. While this is partially related to instrument timing and capture limitations and low overall counts, there is another, more complicated issue. In most PALS measurements, the sample under

analysis constitutes the vast majority of mass in the immediate vicinity of the positron source, because the sample completely surrounds the source on at least one side. In this research, the actual actinide oxide crystals were often less than 2 mm in the major dimension. The most important effect of this is in the reduction of the relative volume of sample compared to stage, though any crystal with areal face dimensions smaller than ~3 × 5 mm will also result in excess air annihilations since the Na-22 source surface area is about this size. Therefore, as will be shown in the results section, the contributions to the lifetime curves by materials other than the test samples dominate, making the measurements of the actinide crystals difficult to resolve. These lifetime curves are the sum of contributions from annihilation lifetimes in the various plastics, organic materials, and the crystals themselves.

In order to try to determine these contributions, the lifetime spectra were plotted against a summed exponential composing of either two or three component terms, depending on whether there was a sample present or not. This was done based on the knowledge that certain materials (air, plastic, and either copper or oxide) were present during the sample runs. Therefore, it was assumed that their contributions should be observed in the tail of the lifetime spectra. These exponentials were convolved with a Gaussian function to account for resolution in the system. The fitting equation is given below as Equation (1) [6].

$$D_f(t) = \sum_{i=1}^{k+1} \frac{I_i}{2} \exp\left[ -\frac{t - t_0 - (\sigma_s^{\,2} / 4\tau_i)}{\tau_i} \right] \left[ 1 - erf\left( \frac{1}{2\sigma_s \tau_i} - \frac{t - t_0}{\sigma_s} \right) \right] \qquad (1)$$

In this equation, $I_i$ is the coefficient representing the contribution from material *i*, $\tau_i$ is the lifetime associated with that material, $\sigma_s$ is the standard deviation of the spectrum's peak (~270 ps in these spectra), and $t_0$ is the offset time (0 for this setup) [6].

The differences between the count values observed in the spectra and those in the fit function are summed to obtain a goodness-of-fit (GooF) value. Then the coefficients of the two or three exponential terms were varied in order to determine where the GooF value was minimized, indicating that the fit is close to the data values. This process was partially automated in MATLAB. Some of these fits will be discussed in the next section.

**Process Review**

A concise summary of the nominal overall collection and analysis process will now be presented. The process begins with the decay of a Na-22 atom, releasing the decay gamma photon and a positron. This positron then annihilates some time later, releasing two annihilation gamma photons. The decay gamma and one of the annihilation gammas deposit energy into the $BaF_2$ crystals (one photon in each detector). This causes scintillation in the crystal, and these scintillation photons cause an electron avalanche in the photomultiplier tubes of the detectors. This avalanche amplification is what becomes the electric signal output of the detectors.

The electrical signal from the each detector is routed via coaxial cable to the oscilloscope, where it is split. One line goes into the input of the scope, while the other goes to the CFD, which in turn generates a square pulse for each of the two signals. These square pulses are routed into a logic AND circuit to detect coincidence; the

coincidence pulse is then routed to the oscilloscope as a trigger signal. Upon receiving this trigger, the scope reaches into its memory and pauses while storing the two waveforms. When the laptop attached to the scope detects this pause, it polls the scope's memory of the waveforms and resets the scope so that it can trigger once again.

Each pair of waveforms is saved as a separate file; a set of tens of thousands of these files makes up the raw data for each spectrum. The files are imported one by one into a MATLAB code, where they are processed for a time difference, which is then recorded as a count in the appropriate bin of a lifetime histogram. This histogram is the spectrum for that source-air-crystal system. The spectrum is then fit against a sum of exponential terms that represent the decay lifetime of each of the material components present. The pre-exponential coefficients for each of these components represent their contributions to the overall system, and in turn should show differences for each crystal tested.

# IV. Analysis and Results

## Overview

This section contains the findings of this research and is split into two main parts. The first part discusses analysis of the raw data and of the fitted data in order to obtain lifetime data for the materials present during each collection period. The second part highlights some additional results, specifically, an inverse correlation between count rate and sample mass and the effect of increase in total counts on data profiles.

## Lifetime Spectra

The average lifetime of positrons in sintered $ThO_2$ pellets is 184 ps as described in [8]. This is exceptionally low for a ceramic material, but not unexpected, since actinides carry with them a large number of electrons. Because a crystalline solid should be much more densely packed than a sintered solid of the same material, the positron lifetime for $ThO_2$ is predicted to be between 160 and 180 ps; for the exponential fits, the value of 180 ps was used. While no defect-free crystal of $ThO_2$ was available to test, by taking lifetime spectra of multiple crystals was expected to produce a representative set of data for crystals of varying quality. Uranium-doped thoria ($U:ThO_2$) was also analyzed to identify any distinct differences; in particular, if the uranium incorporates interstitially, it should noticeably decrease the positron lifetime.

Since the exact number of counts taken was different for each sample, a direct comparison of counts per lifetime bin has no meaning on the graphs presented here. That is, a graph of raw counts for a data set with 16,000 counts would plot above one with 10,000 counts regardless of the average lifetime. Therefore, the data are normalized to

whichever bin contained the most counts. Therefore the graphs show a peak value of 1 in this bin. The value in this construct is that it compares the proportion of annihilations with lifetimes in the range of that bin, though in all cases the sample peaks ranged 100-200 ps, not surprising given the resolution of the oscilloscope. The normalized data preserves the relative values of the data (since it is a simple distributed division), and so it is used both for comparisons and again later on, when fitting the data to an exponential decay function.

Once the final 'trapeze' configuration for the PALS systems was established, a number of baseline measurements were taken. The first such data set was for the system with no Na-22 source present, which resulted in a relatively low number of counts, as expected. The data have a very short and sharp time peak, which is also expected; the primary source of gamma coincidences in this case are photons that Compton scatter from one detector into the other, and this is a nearly instantaneous process. Though the lead sheet between the detectors reduced these occurrences by about two-fifths, they are still present and accounted for about 6% of the counts even with the source present. The data are graphed in Figure 15.

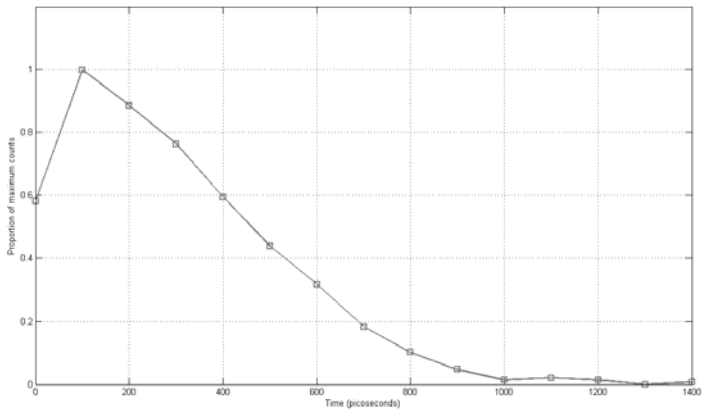


**Figure 15: The background spectrum for the PALS system with no source present.**

The next baseline measurement was taken with the T-134Q Na-22 sandwich source on the stage, but with no crystal or other sample placed on top of it. This measurement is expected to show a higher average lifetime, a 'fatter' tail, than an analysis run. The reason for this is that the annihilations in the plastic and organic materials will be contributing a larger fraction of the lifetime spectrum than they would with a sample present. The average lifetime in these materials is far longer than in the actinide samples due to their low electron density. This is mainly a property of their atomic makeup, though the microstructure of the paper is porous as well. In addition, a significant number of positrons will annihilate in the air above the stage, instead of in the sample that would normally be there. The average lifetime in air is far longer than in any form of condensed matter.

The final baseline measurement was taken with a relatively large (approx. 10 × 10 × 1 mm) piece of copper sheeting on top of the source. Since the average lifetime of copper is well-known, this collection was intended to act as a calibration and

quantify error. In general, the average positron lifetime in $ThO_2$ is expected to be higher than in copper, since the valence electrons in copper are far more mobile and its apparent electron density is higher. Therefore, the data set with no sample and the data set with the copper sheet provide reasonable upper and lower bounds for the system. These data are graphed together in Figure 16, along with the background spectrum for comparison purposes. The measured copper positron lifetime spectrum lies above that of the stage alone in the 200 ps bin; this is unusual since the copper sample system overall should have a lower average lifetime. The most likely explanation for this anomaly is that there was a probabilistic clustering in that bin that would not be observable with a larger data set; that is, more counts should shift the peak back into the 100 ps bin where it was expected to fall.

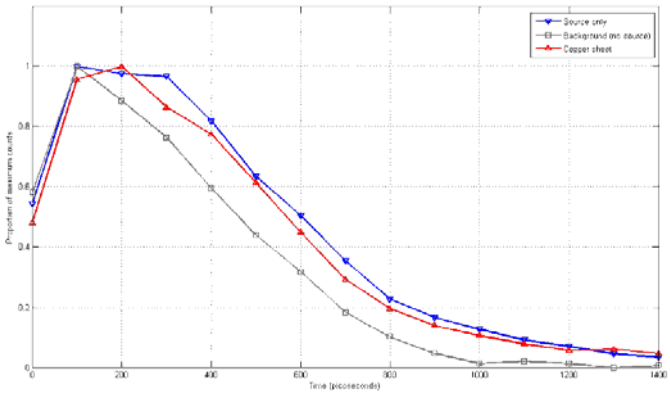


**Figure 16: Lifetime spectra taken with no sample on the stage and with the copper plate sample present. These spectra will act as upper and lower bounds for the crystal spectra.**

AFIT possesses a large number of very small actinide oxide crystals, with about 80 catalogued. Most of these are about the size of a grain of sand, but there are a few larger samples. The samples selected for this research were those that are larger (in order

to cover more of the Na-22 source), or those that appear especially transparent and thus are likely to contain fewer light-scattering defects. Nine crystals were analyzed, to include five $ThO_2$ samples and four U:$ThO_2$ samples. Lifetime spectra for each of these crystals are presented in the following figures, with the two bounding data sets to provide a reference.

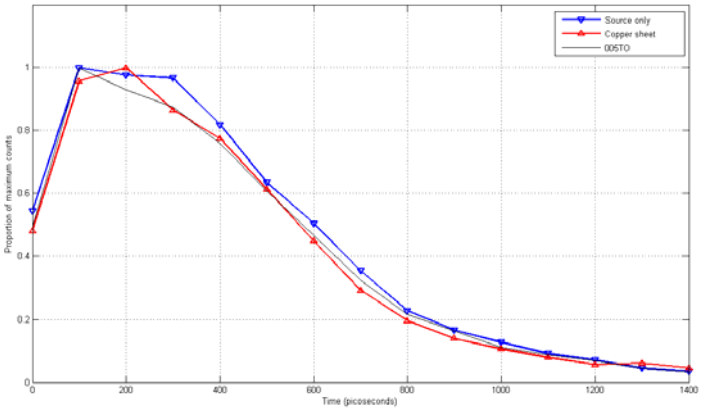


**Figure 17: Lifetime spectra for 005TO with bounding reference spectra.**

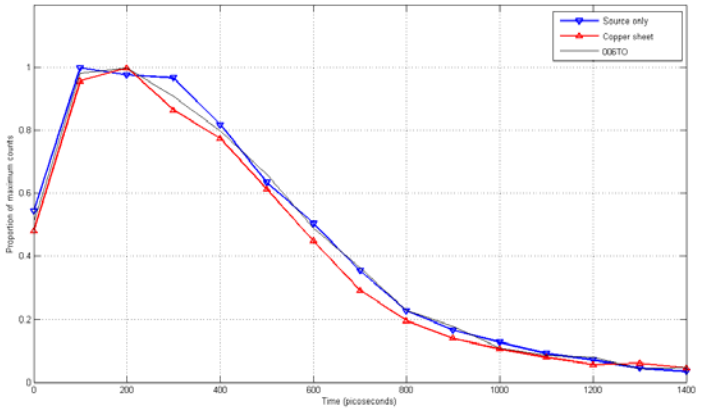


**Figure 18: Lifetime spectra for 006TO with bounding reference spectra.**

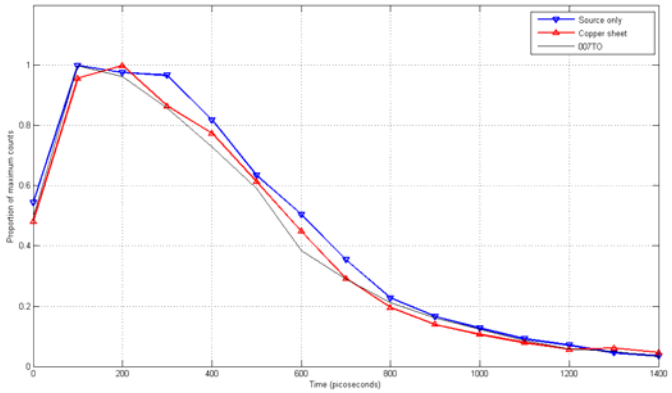


**Figure 19: Lifetime spectra for 007TO with bounding reference spectra.**

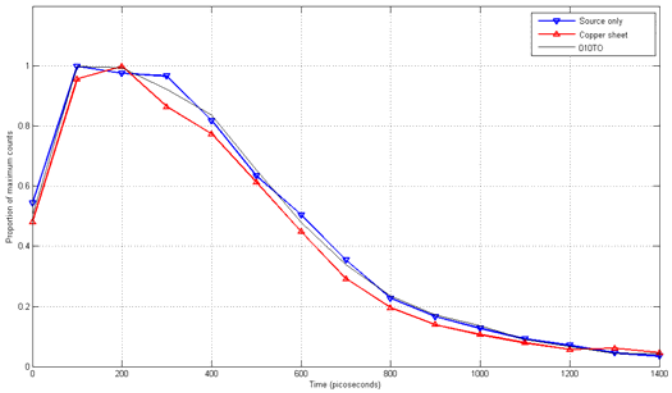


**Figure 20: Lifetime spectra for 010TO with bounding reference spectra.**

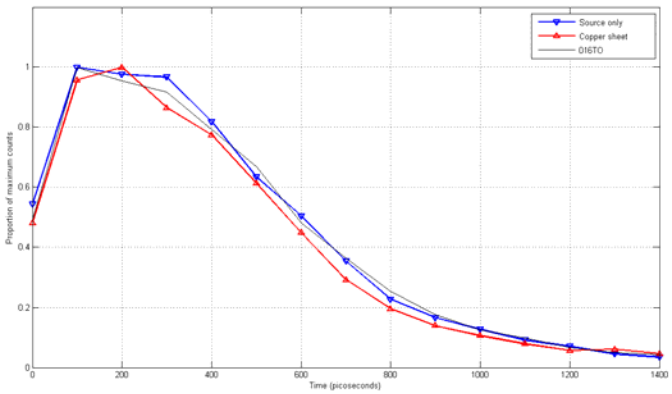


**Figure 21: Lifetime spectra for 016TO with bounding reference spectra.**

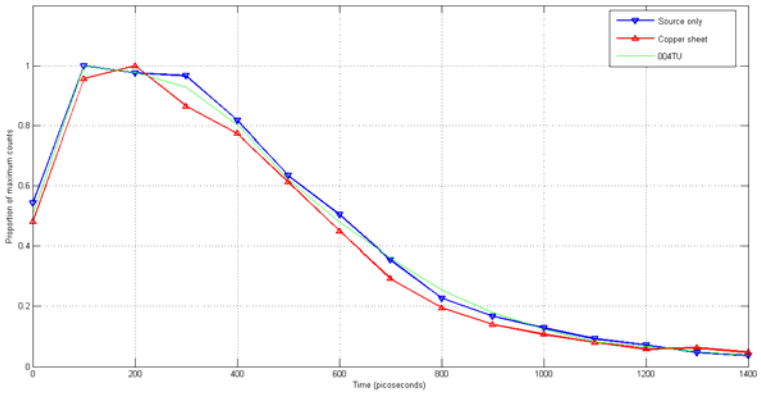


**Figure 22: Lifetime spectra for 004TU with bounding reference spectra.**

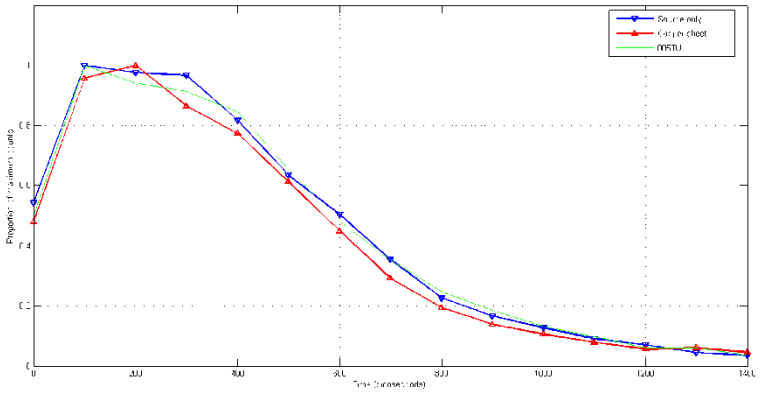


**Figure 23: Lifetime spectra for 005TU with bounding reference spectra.**

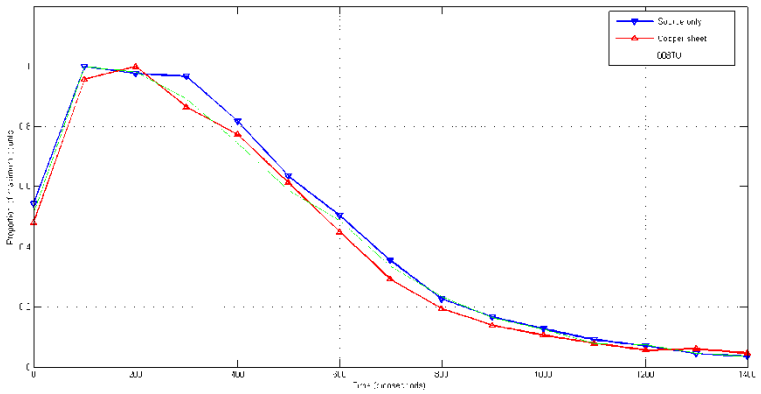


**Figure 24: Lifetime spectra for 008TU with bounding reference spectra.**

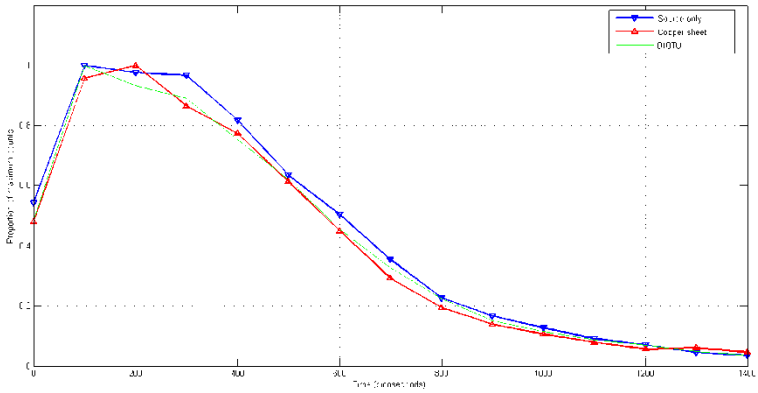


**Figure 25: Lifetime spectra for 010TU with bounding reference spectra.**

It is worth looking for specific trends in the data, to see if there are distinct signatures for either material. The following figures present the entire range of lifetime spectra for each of the two crystal types individually, followed by a figure showing the two groups graphed against each other. Once again, the two bounding data sets are provided for reference.

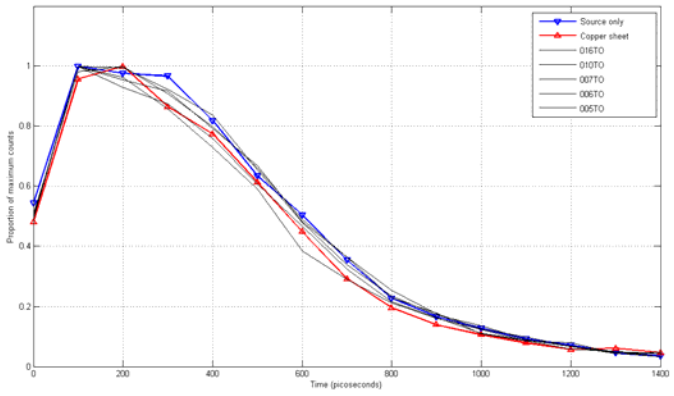


**Figure 26: Collected spectra for all $ThO_2$ crystal samples.**

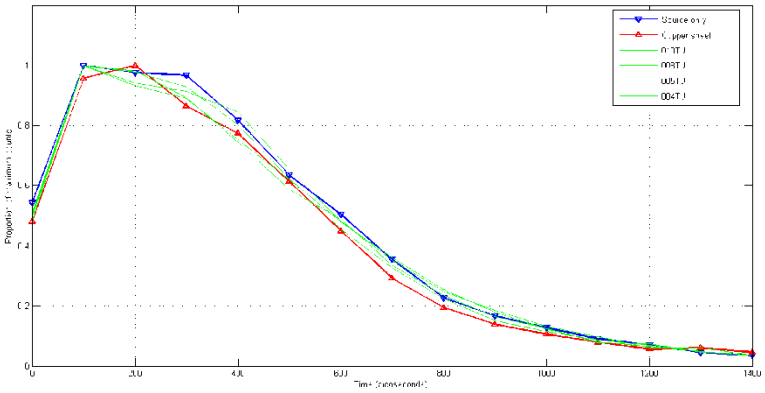

**Figure 27: Collected spectra for all U:$ThO_2$ crystal samples.**

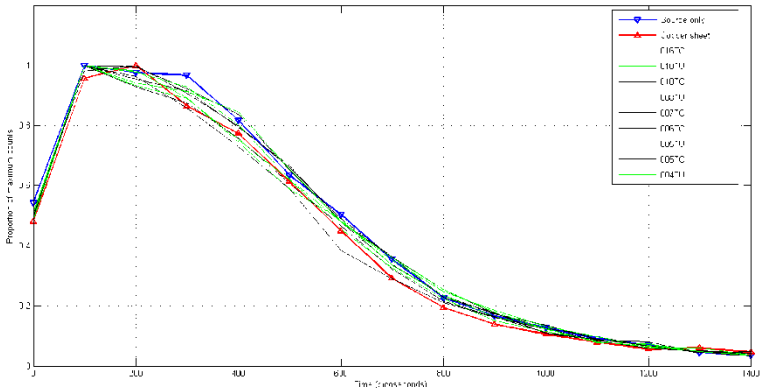

**Figure 28: Collected spectra for all crystal samples, with color indicating whether the sample is $ThO_2$ or U:$ThO_2$.**

While all of the lifetime curves were close to where they were expected to fall (in between the bounding curves), there are many individual points that fall outside these expectations. Further, there is no clear grouping of crystals by elemental makeup or other characteristic. In any case, it is certainly true that specific signatures are not readily apparent. The same result emerges under quantitative analysis; no one group of crystals consistently shows higher or lower lifetime differences (from the bounding functions) than another. It is expected that a pattern or signatures will emerge if the crystals'

contributions to the spectra can be enhanced; this may be possible with a greater count rate, a less massive stage (or sample holder), and/or larger crystal samples.

To that end, it was decided to separate the different decay components using the raw data, since the back end of a lifetime spectrum will reflect contributions from all materials present. This involved fitting a two- or three-term exponential decay function convolved with a Gaussian resolution function and obtaining a goodness-of-fit.

The figures below present results of functional fits to the raw data. While the fitting does not give enough detail to show specific lifetime signatures for the crystals, it lends credit to the idea that there are specific lifetime contributions from the materials. These fitting curves assumed two lifetime components without a sample or three components with a sample (air, plastic, and sample if present). Each coefficient is divided by the sum of all coefficients to give an estimate of contribution to the overall spectrum.

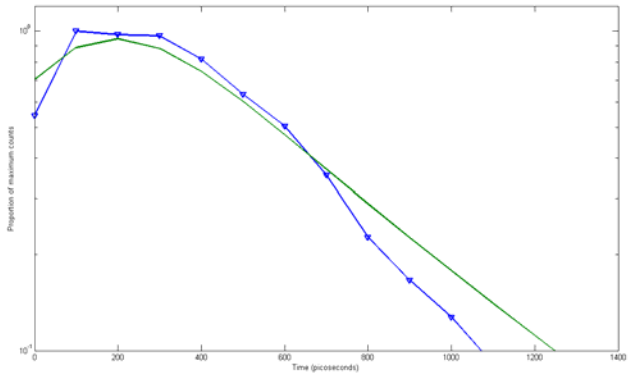


**Figure 29: Exponential/Gaussian fit for source only data. The estimated contributions from each component are 46.8% from air and 53.2% from plastic.**

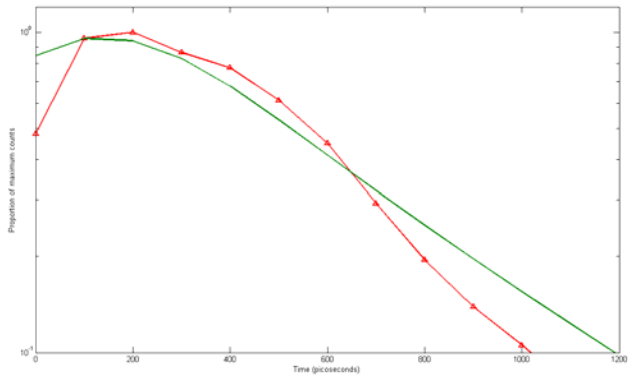

**Figure 30: Exponential/Gaussian fit for copper sheet data. The estimated contributions from each component are 45.9% from air, 39.0% from plastic, and 15.1% from copper.**

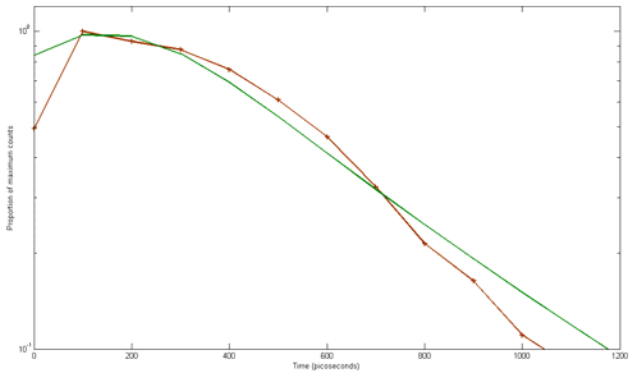

**Figure 31: Exponential/Gaussian fit for 005TO data. The estimated contributions from each component are 42.1% from air, 35.5% from plastic, and 22.4% from $ThO_2$.**

These fits indicated a large lifetime contribution from longer-lifetime materials. Therefore, it was decided to try fitting only to the far end of the lifetime curve in the 600-1400 ps range to try to see if there was a single long lifetime term that was dominating. These fits also used Equation (1), but with only a single term instead of three. One such fit is shown in Figure 32.

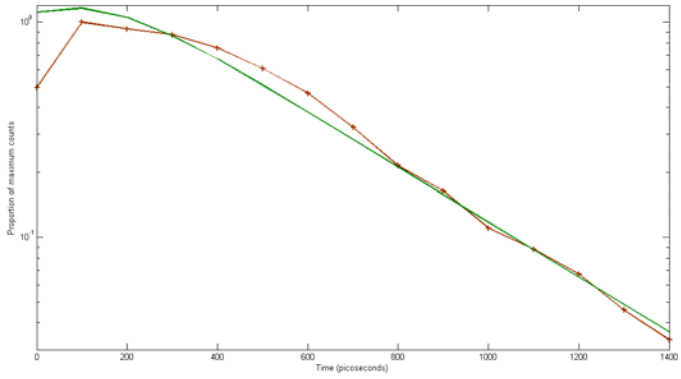


**Figure 32: Exponential/Gaussian fit to the tail (600-1400 ps range) of the 005TO data. The single lifetime for this fit curve is 340 ps.**

All the lifetime spectra showed a close fit to single lifetimes between 320 and 360 ps. This supports the indication from the multi-material fit that longer lifetime materials are have a large influence on the shapes of the curves, and may be drowning out the lifetime contributions of the crystals. Given the geometry of the setup, air is the most likely material contributing to this result, with some contributions from plastic also represented. This is discussed further in the next section.

## Additional Analysis and Results

Upon examining the data as a whole, an additional result seemed to emerge that may indicate unexpected positron interactions or mass dependencies. It appears that the count rate for the apparatus used in this research was nearly directly related to the mass of the sample placed on the stage. This relationship is shown in Figure 33, and the data is given in Appendix B.

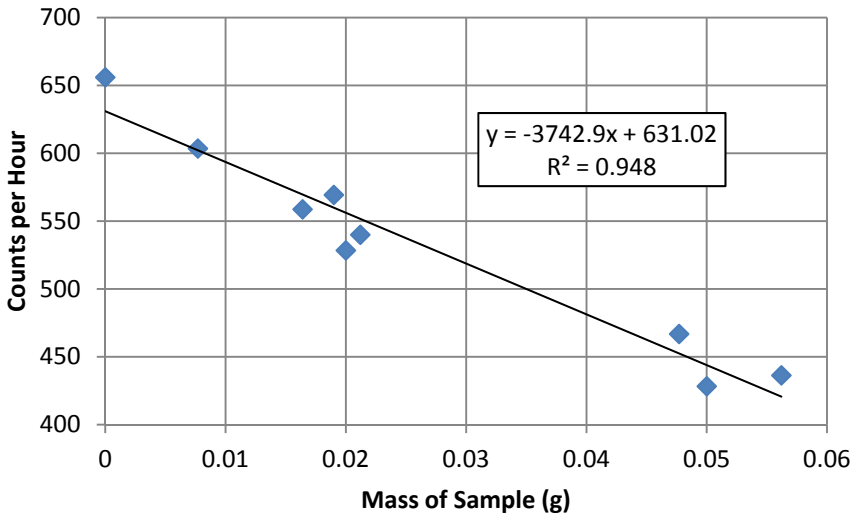


**Figure 33: Linear relationship between the mass of sample and count rate.**

At first, it was thought that this phenomenon resulted from self-shielding by the sample. However, a much more likely explanation is that air annihilations above the sample were being added to the counts. None of the crystals examined were large enough to cover the Na-22 salt deposit inside the source, so in all cases there were some positrons that were emitted upwards but did not encounter the crystal at all. These positrons annihilate in air, and the events were closer to the detectors (which were above the sample stage) and thus increased the likelihood of being captured via an increase in their solid angle. Thus, their contributions to the spectra are represented disproportionately. This process is show graphically in Figure 34.

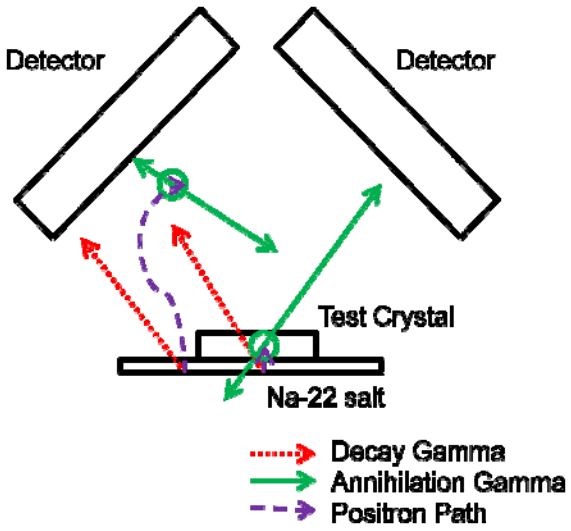


**Figure 34: Schematic showing preferential detection of air annihilations due to incomplete coverage of source salt.**

As part of the final data analysis, an attempt was made to determine a true number for the required counts to produce a spectrum. One million is commonly quoted as the needed number, and was used as a guide when conducting this research. Krause-Rehberg suggests the required minimum is as high as five million counts [6]. This research fell far short of that number, but tens of thousands of counts is not insignificant either. To test the validity of the sample size obtained for these crystals, lifetime spectra were generated using the first 100, 1,000, 10,000, and 20,000 data points from one single run of the system. This was expected to show how many points would be needed to converge to a consistent set of free parameters in the fitting of the spectrum obtained using the full 29,657 measurements taken for this crystal (005TO). This crystal measurement was chosen since it of the larger data sets captured, 005TO is one of the largest available crystals, and the spectrum shape is one of the closest to expectations. The spectra, which are really from the same data set, are shown in Figure 35.

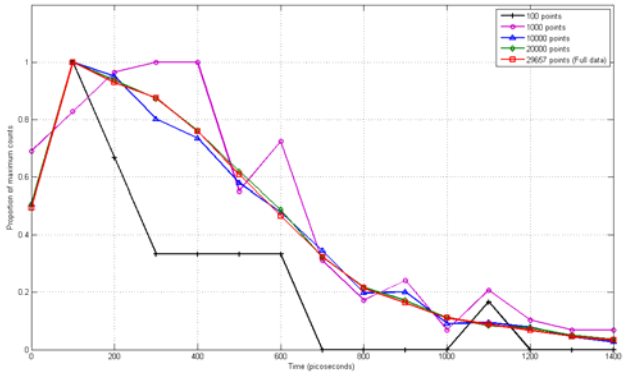


**Figure 35: Lifetime spectrum for 005TO showing the effects of reduced counts.**

Very small numbers of counts (100 or 1,000) deviate wildly from the full spectrum, but even with 10,000 counts the final shape begins to emerge. There is almost no discernible difference between the spectra generated from 20,000 counts and the full 29,657 counts; the average difference in individual bins is about 1%. Therefore, 20,000 counts are sufficient for this setup. However, if the sampling rate was increased or interpolation successfully implemented, 20,000 total counts would be split into more bins, and that could once again distort the data. A better measure of sufficiency is the number of counts in the peak bin, which was 1,803 for this case of 10 GS/s and 20,000 total counts. The end result is that ~2,000 counts in the peak bin is the minimum to start to establish the correct lifetime fitting spectrum.

# V. Conclusions and Recommendations

## Conclusions

Overall, the research was not successful. The data and subsequent analysis did not allow any definite conclusion to be drawn about the absolute or relative quality of the crystals. However, there were a number of accomplishments as a result of this effort that are valuable either on their own or as a precursor to follow-on research. A conceptually sound PALS system was constructed, to include the assembly of a positron source specialized for PALS. This system was used to analyze several crystal samples, providing a baseline for subsequent PALS work with thorium dioxide, uranium-doped thorium dioxide, and uranium dioxide single crystals. Furthermore, the lessons learned in the course of this thesis will prove very valuable for future researchers conducting PALS on any material, since the lifetime spectrometer's configuration was not tailored to any specific material or sample configuration, a limitation that was common in previous research.

Despite the effort made in designing, constructing, and troubleshooting the apparatus, the data it yielded did not clearly show distinct lifetime signatures, and thus it was impossible to draw any precise conclusions from the spectra regarding crystal quality. Therefore, examination and critique of the whole process was conducted in order to ensure the maximum value of the research effort. The results of this critique are presented in the remainder of this document.

Despite attempts to minimize extraneous annihilations in other materials, many of the lifetime data points seem to have been in the various organic materials in the stage

and air. A related issue is that the crystals were extremely small. This is in addition to the fact that ~1/2 of the positrons will be lost due to their emission from the bottom of the stage. Lost positrons reduce the overall counts measured, which in turn makes discernment of unique lifetime signatures much more difficult. There is some reason to suspect that the use of $BaF_2$ detectors is problematic as they do not completely obey the classic voltage response curves expected from scintillators (such detectors are normally operated in a stable response region which was not observed during setup testing). The PMTs also introduce some timing uncertainty even when functioning perfectly, which is known and indicated in the manufacturer's documentation. Finally, the interpolation and analysis methods may have introduced additional error into the data.

The research fell short of the goal of creating a library of lifetime spectra that provides detailed data about the quality and growth conditions of the existing actinide oxide crystals. This, in turn, means that any new crystals that are grown cannot be analyzed for comparison with the old samples. Until a clear and repeatable signature for each individual crystal can be elicited from its PALS data, this goal will remain unfulfilled.

**Future Work**

Despite the difficulties encountered, there is a great deal of potential for follow-on work based on the lessons learned during this research. The single most important improvement would be to improve the sampling rate. This would allow the fits to be made more accurately. An oscilloscope with a higher sampling rate, or finding a way to link multiple scopes with a common timing system, would improve these results. This

would necessitate an increase in the number of counts to make sure the lifetime is accurately represented. That increase should be at least equivalent to the increase in sampling rate.

Hardware improvements may be the easiest to implement. Larger actinide oxide crystals would have improved the sample fraction of annihilations. Parallel AFIT research into hydrothermal growth was stalled and was not able to provide crystals in the 5 to10 mm nominal sizes, which would be well suited to PAS analysis. Fortunately, this growth work is likely to continue, though the idea of cutting such a crystal in half to allow for surrounding of the positron source may not be feasible since the crystals are radioactive. It may also be possible to further remove material from the surroundings of the positron source to cut down on extraneous annihilations. Moving the entire system into a lower-background area will reduce background counts, and conducting the lifetime analyses in a vacuum would eliminate the air annihilation contribution. In addition, the detectors may be improved, whether by increasing the solid angle (perhaps by using a third detector) or moving to a faster photomultiplier technology. Finally, a more active source may be used; this could be obtained directly or assembled using the procedure validated during this research, possibly with a reduced isotope deposition area. An alternate solution may be to use AFIT's slow positron beam, though this instrument will only be set up for DBAR and ACAR measurements for the foreseeable future.

Software improvements are possible too. An obvious issue with the data collection method is the large amount of disk space that it occupies. If the method is to be scaled up, some way to reduce file size must be found; perhaps by eliminating the recording of noise on either side of the pulses. A better interpolation scheme may yield

better lifetime data, though without increasing sampling rate it will be difficult to verify that the interpolated data is really more accurate. Lastly, improving the algorithm for extracting average positron lifetimes from the binned data would be helpful, but if the counts can be increased greatly and the interpolation yields very finely binned data, it should be possible to use an existing analysis tool such as PALSfit.

## Appendix A: List of Components and Settings

| Name/Model Number | Designation Number | Settings |
|---|---|---|
| Tektronix DPO 7104 Digital Phosphor Oscilloscope | B022288 | Display traces:<br>C3 300 mV/div 50 Ω<br>C4 300 mV/div 50 Ω<br>Trigger:<br>C2 neg. trigger -380 mV<br>Time settings:<br>10 ns/div 10.0GS/s 100 ps/pt |
| BICRON model 1.103M787BAF2/2L-X Barium Fluoride Detectors | 60007-1338<br>60007-1343 | |
| ORTEC 4006 Minibin & Power Supply | 440 | |
| ORTEC 556 High Voltage Power Supply | 4200 | -2800 V |
| ORTEC 935 Quad CFD | 06215297 | Threshold: -25mV |
| ORTEC CO4020 Quad 4-Input Logic | 07310281 | |
| Resistive Pass-throughs (found on the rear of ORTEC 480 Pulser) | | 50 Ω |
| Dell Latitude E6510 Laptop | 5703 | Windows 7 Professional |
| Western Digital 3200ME-01 External Hard Drive | WXEY08AA5873 | |
| LabView Software | | Library file:<br>Halstead_RecordSingleWaveform.llb<br>Visual interface file:<br>VanDyk_TriggerToFile_v3.vi |

## Appendix B: List of Data Collection Runs Presented in the Main Document

| Data date | Source | Sample | Configuration | Run Time (h) | Counts | Counts/Hour | Sample Mass (g) |
|---|---|---|---|---|---|---|---|
| 2-Dec | none | none | Trapeze Angled, big BaF2 (-2800V), lead plate | 23.28333 | 786 | 33.75805 | |
| 3-Dec | PEEK sandwich | none | Trapeze Angled, big BaF2 (-2800V), lead plate | 24.83333 | 16291 | 656.0134 | 0 |
| 4-Dec | PEEK sandwich | 007TO | Trapeze Angled, big BaF2 (-2800V), lead plate | 23.88333 | 10422 | 436.3712 | 0.0562 |
| 5-Dec | PEEK sandwich | 010TU | Trapeze Angled, big BaF2 (-2800V), lead plate | 94.91667 | 54040 | 569.3415 | 0.019 |
| 9-Dec | PEEK sandwich | 010TO | Trapeze Angled, big BaF2 (-2800V), lead plate | 25.06667 | 13535 | 539.9601 | 0.0212 |
| 10-Dec | PEEK sandwich | 008TU | Trapeze Angled, big BaF2 (-2800V), lead plate | 24.1 | 13465 | 558.7137 | 0.0164 |
| 11-Dec | PEEK sandwich | 016TO | Trapeze Angled, big BaF2 (-2800V), lead plate | 23.7 | 12446 | 525.1477 | |
| 12-Dec | PEEK sandwich | 005TU | Trapeze Angled, big BaF2 (-2800V), lead plate | 23.65 | 12498 | 528.4567 | 0.02 |
| 13-Dec | PEEK sandwich | 005TO | Trapeze Angled, big BaF2 (-2800V), lead plate | 71.66667 | 30696 | 428.3163 | 0.05 |
| 16-Dec | PEEK sandwich | 004TU | Trapeze Angled, big BaF2 (-2800V), lead plate | 23.55 | 14214 | 603.5669 | 0.0077 |
| 17-Dec | PEEK sandwich | 006TO | Trapeze Angled, big BaF2 (-2800V), lead plate | 23.65 | 11042 | 466.8922 | 0.0477 |
| 18-Dec | PEEK sandwich | Cu plate | Trapeze Angled, big BaF2 (-2800V), lead plate | 36.36667 | 11318 | 311.2191 | |

**Appendix C: Na-22 Positron Source Assembly Procedure**

# $^{22}$Na Deposition onto Polymer Films: Radiation Test Plan

# (1 November 2013)

Capt Edward C. Schneider

*Air Force Institute of Technology, Wright-Patterson AFB, OH 45431*

## I. INTRODUCTION

This document discusses in details the steps and procedures required to complete $Na^{22}$ deposition on to thin plastic film. This document also addresses the deposition of $Na^{22}$ sandwiched between two 10 mm x 10 mm x 8 um PEEK plastic film samples. All radioactive handling of materials will be conducted within the radiation hood located in the chemical lab in building 470 at Wright Patterson AFB OH. The $^{22}$Na source (T-134) will be deposited from their containers on to the film to make a radioactive sandwich source.

The entire solution of the radioactive NaCl will also be placed on two PEEK plastic film samples. The samples will be heated to ~80$^{\circ}$C to enhance water evaporation and accelerate the Na-22 deposition. Following the evaporation period, the plastic samples will be placed on top of the other to form a sandwich configuration. Tape and aluminum foil will secure the sample and in particular ensure no radioactive leakage. Through entire process a Geiger counter (or other form of a radioactive counter) will be used to monitor activity. All radioactive waste will be disposed of properly and all functional radioactive materials will be properly labeled for future safety and verification.

## II. TEST OBJECTIVES

The objective for this test is to safely deposit approximately 20 drops of $Na^{22}$ solution onto the PEEK samples.

1) Plastic film Samples Radioactive Deposition

    a. Perform outlined objectives without radioactivity to confirm methodology

    b. Drip 20 drops onto two 10 mm x 10 mm x 8 um near identical plastic film samples

    c. Heat sample at 80$^{\circ}$C to evaporate water

d. Place PEEK plastic film samples on top of each other (sandwich configuration) and secure with tape

e. Scan room for activity to distinguish between radioactive contamination and nonradioactive laboratory waste.

2) Dispose of all radioactive and nonradioactive waste appropriately. Properly label functional radioactive material for safety and future verification.

## III. PROPOSED SCHEDULE

All test objectives will be completed 12 November 2013.

## IV. TEST PRIORITY

If time permits, all outlined tests will be conducted. Due to possible unforeseen equipment failures and scheduling issues the priority of measurements is exactly as numbered in the test objectives section of this test plan, excluding Objective 2 radioactive disposal, which must be accomplished. Timeline may be extended if necessary.

## V. TEST SETUP

In order to perform described measurement the following equipment will be required.

1) $^{22}$Na T-134 1.7 uCi (1 Feb 2013)
2) Two 10 mm x 10 mm x 8 um PEEK plastic film samples
3) Single Sided Tape
4) Multiple 22 Gauge Syringes
5) Lead Bricks

6) 1 Hot Plate. Make sure to cover hot plates with aluminum foil in order to further separate hot plates from radioactive material. Do not make Al foil disruptive to handling material on top as well as temperature knobs in front.

7) Labeled Radioactive Waste Container

8) Transfer Tools: Syringes, scissors

9) Gloves, Laboratory Coats, and Goggles

10) Radiation Detector

11) Radioactive waste container (plastic bag with the opening rolled over the edge of its support container)

12) Transfer tools to include tweezers and syringes

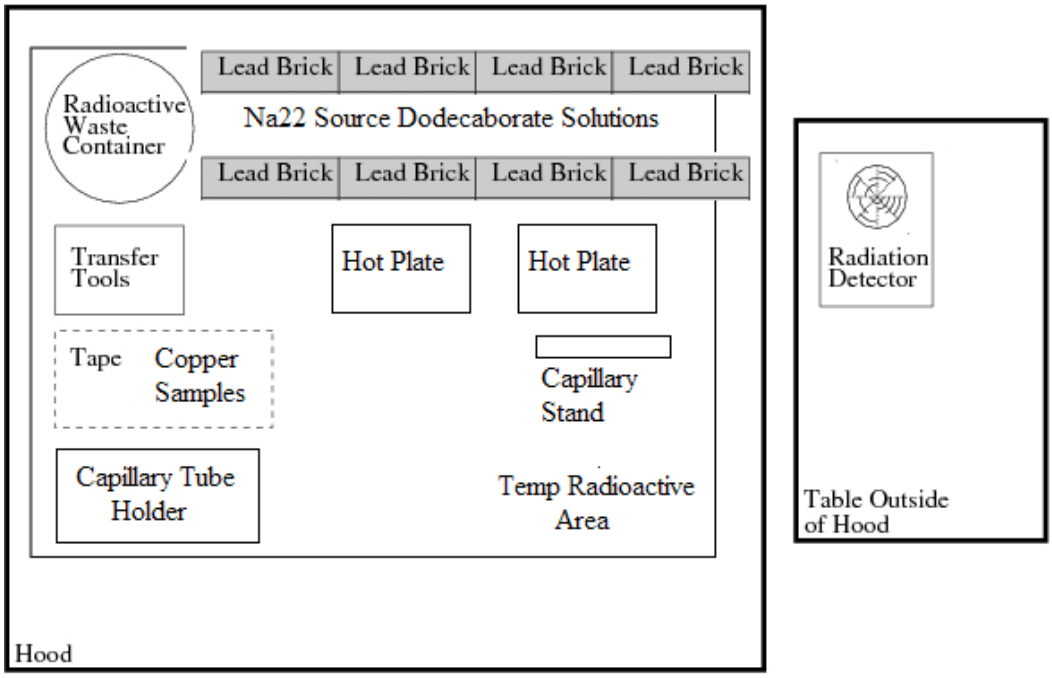

## VI. TEST PROCEDURES

1) Plastic film Samples with radioactive $^{22}Na$ will be made by dripping radioactive solution onto a 10 mm x 10 mm x 8 um plastic film sample placed on top aluminum foil wrapped around a hot plate. Following evaporation, samples will be placed on single sided tape and then sandwiched together. Detailed procedures are:

    a. Perform outlined objectives without radioactivity to confirm methodology. Make any changes to the procedure based on dry runs prior to continuing.

    b. Bring out two 10 mm x 10 mm x 8 um plastic film sample and place on top of left most hot plate covered in aluminum foil.

    c. Bring out a single $^{22}Na$ source vial from in-between the lead bricks at the far end of the hood and gently remove cap.

    d. Insert syringe into $^{22}Na$ source and draw 0.3-0.5 mL of solution.

    e. Gently drip solution on top of 10 mm x 10 mm x 8 um plastic film samples, which are on the hot plate heated to 80 $^{o}C$.

    f. Allow drops to evaporate, on the order of 1-2 minutes.

    g. Repeat c-f until all the liquid is gone from the syringe and the entire solution is gone.

    h. Place syringe onto temporary radioactive area and put $^{22}Na$ source back in-between lead bricks.

    i. Cool samples, and place on single sided tape.

    j. Place plastic film samples together in a sandwich configuration and secure with tape additional tap.

    k. Cut edges and affirm with swipes no radioactive materials are present. If radioactivity is present, dispose of in the radioactive waste container.

    l. Scan room for activity to distinguish between radioactive contamination and nonradioactive laboratory waste.

2) Dispose of all radioactive and nonradioactive waste appropriately. Properly label functional radioactive material for safety and future verification.

## VII. SPECIAL REQUIREMENTS

When dealing with radioactive materials, care must be taken to limit exposure. Before handling any radioactivity make sure to follow ALARA (As Low As Reasonably Achievable) procedures. For experimentation two pairs of gloves and coat are required to prevent exposure to skin. Laboratory goggles are also required to prevent exposure to the eyes. All radioactive handling requires at least two people to be present in order to provide additional resources to ensure safety. In case of glove contamination, remove one pair of gloves using single finger and dispose of contaminated glove in the radioactive waste bag.

## VIII. POINTS OF CONTACT

The following people can be contacted should any questions arise.

Capt Edward C. Schneider, E-Mail: edward.schneider@afit.edu

Dr. James Petrosky, E-Mail: james.petrosky@afit.edu

## Bibliography


[1] J. M. Mann, *Hydrothermal Crystal Growth of Tetravalent and Pentavalent Metal Oxides,* Clemson, SC: Dissertation (Ph.D.)--Clemson University, August 2009.

[2] W. D. Kingery, H. K. Bowen and D. R. Uhlmann, Introduction to Ceramics, New York: Wiley-Interscience, 1976.

[3] K. S. Krane, Introductory Nuclear Physics, Hoboken, NJ: John Wiley & Sons, 1988.

[4] D. R. Lide, CRC Handbook of Chemistry and Physics, Boca Raton: CRC Press, 2004.

[5] J. J. Graham, *Hydrothermal Crystal Growth of Lithium Tetraborate and Lithium Gamma-Metaborate/AFIT/NUCL/ENP/14-M-12,* Wright-Paterson AFB: Thesis (M.S.)--Air Force Institute of Technology, 2014, March 2014.

[6] R. Krause-Rehberg and H. Leipner, Positron Annihilation in Semiconductors, Berlin: Springer-Verlag, 1999.

[7] C. S. Williams, *Three-Dimensional Positron Annihilation Momentum Measurement Technique Applied to Measure Oxygen-Atom Defects in 6H Silicon Carbide,* WPAFB, OH`: Dissertation (Ph.D.)--Air Force Institute of Technology, 2010, March 2010.

[8] D. D. Upadhyaya, R. V. Muraleedharan, B. D. Sharma and K. G. Prasad, "Positron lifetime studies on thorium oxide powders," *Philosohical Magazine A,* vol. 45, no. 3, pp. 509-518, 1982.

[9] M. C. Lindsay, *Set-up and operation of digital PAL spectrometer,* WPAFB, OH: Air Force Research Laboratory - Memorandum for Record, April 2009.

[10] S. Fagan-Kelly, *Three-Dimensional Positron Annihilation Momentum Spectroscopy of Lithium Tetraborate Crystals/AFIT/NUCL/ENP/GNE-13M,* WPAFB, OH: Thesis (M.S.)--Air Force Institute of Technology, 2013, March 2013.

[11] S. M. Jiminez, *Design and characterization of a three-dimensional positron annihilation spectroscopy system using a low-energy positron beam/AFIT/NUCL/ENP/12-M04,* Wright-Patterson AFB, OH: Thesis (M.S.)--Air Force Institute of Technology, 2012, March 2012.

[12] R. C. Slaughter, *Positron Annihilation Ratio Spectroscopy (PsARS) Applied to Positronium Formation Studies,* WPAFB, OH: Thesis (M.S.)--Air Force Institute of Technology, 2010, March 2010.

[13] A. C. Walker, *Positron Annihilation Ratio Spectroscopy Study of Electric Fields Applied to Positronium at Material Interfaces,* WPAFB, OH: Thesis (M.S.)--Air Force Institute of Technology, 2011, March 2011.

[14] C. Ganguly and R. N. Jayaraj, Characterization and Quality Control of Nuclear Fuels, New Delhi: Allied Publishers Pvt Ltd, 2004.

# REPORT DOCUMENTATION PAGE

*Form Approved*
*OMB No. 0704-0188*



**PLEASE DO NOT RETURN YOUR FORM TO THE ABOVE ADDRESS.**

| 1. REPORT DATE *(DD-MM-YYYY)* | 2. REPORT TYPE | 3. DATES COVERED *(From - To)* |
|---|---|---|
| 27 Mar 2014 | Master's Thesis | Aug 2012 - Mar 2014 |

**4. TITLE AND SUBTITLE**

Positron Spectroscopy of Hydrothermally Grown Actinide Oxides

**5a. CONTRACT NUMBER**

**5b. GRANT NUMBER**

**5c. PROGRAM ELEMENT NUMBER**

**6. AUTHOR(S)**

Schneider, Edward C, Capt, USAF

**5d. PROJECT NUMBER**

JON 14P334B

**5e. TASK NUMBER**

**5f. WORK UNIT NUMBER**

**7. PERFORMING ORGANIZATION NAME(S) AND ADDRESS(ES)**

Air Force Institute of Technology
Graduate School of Engineering and Management (AFIT/EN)
2950 Hobson Way
Wright-Patterson AFB OH 45433-7765

**8. PERFORMING ORGANIZATION REPORT NUMBER**

AFIT-ENP-14-M-33

**9. SPONSORING/MONITORING AGENCY NAME(S) AND ADDRESS(ES)**

Department of Homeland Security / Domestic Nuclear Detection Office
William Ulicny
12th & C Street SW
Washington, DC 20024
William.Ulicny@dhs.gov

**10. SPONSOR/MONITOR'S ACRONYM(S)**

DNDO

**11. SPONSOR/MONITOR'S REPORT NUMBER(S)**

**12. DISTRIBUTION/AVAILABILITY STATEMENT**

DISTRIBUTION STATEMENT A.
APPROVED FOR PUBLIC RELEASE; DISTRIBUTION IS UNLIMITED.

**13. SUPPLEMENTARY NOTES**

This material is declared a work of the U.S. Government and is not subject to copyright protection in the United States.

**14. ABSTRACT**

In recent years AFIT has built expertise and resources dedicated to the growth and characterization of actinide oxides. The primary purpose of this research was to integrate positron spectroscopy – with which AFIT also has a long history – into this actinide research. The main objectives were to construct a Positron Annihilation Lifetime Spectroscopy system, including a new positron source, and to characterize a number of hydrothermally grown ThO2 and U:ThO2 crystals. Lifetime measurements were conducted on nine crystal samples and the spectra analyzed to determine the purity and quality of the crystals. In addition, analysis and fitting of the experimental data allowed estimates of contribution percentages to be made; the samples themselves account for less than 30% of the sample counts in all cases. Overall, the low resolution and large number of non-sample counts indicates that the system was not sufficient to characterize the crystals. A strong foundation for actinide PALS studies was laid, but further work is required to build a more effective system.

**15. SUBJECT TERMS**

Positron Spectroscopy, PALS, Thorium Dioxide, Uranium Dioxide

| 16. SECURITY CLASSIFICATION OF: | | | 17. LIMITATION OF ABSTRACT | 18. NUMBER OF PAGES | 19a. NAME OF RESPONSIBLE PERSON |
|---|---|---|---|---|---|
| a. REPORT | b. ABSTRACT | c. THIS PAGE | | | Dr. James C. Petrosky, AFIT/ENP |
| U | U | U | UU | 73 | 19b. TELEPHONE NUMBER *(Include area code)* (937) 255-3636 x4562 James.Petrosky@afit.edu |